21907

İSTANBUL TEKNİK ÜNİVERSİTESİ ⋆ FEN BİLİMLERİ ENSTİTÜSÜ

DAİRESEL SİLİNDİRDEN OLUŞAN İZ AKIŞININ AYIRICI LEVHA İLE PASİF KONTROLU : VİSKOZ VIC BENZEŞİMİ

Yüksek Lisans Tezi

Aydın MISIRLIOĞLU , Müh.(İTÜ)

Ana Bilim Dalı : UÇAK MÜHENDİSLİĞİ

Programı : UÇAK MÜHENDİSLİĞİ

ŞUBAT 1992

ISTANBUL TECHNICAL UNIVERSITY ⋆ INSTITUTE OF SCIENCE AND TECHNOLOGY

PASSIVE CONTROL OF WAKE FROM A CIRCULAR CYLINDER WITH A SPLITTER PLATE : VISCOUS VIC SIMULATION

M.Sc. THESIS

Aydın MISIRLIOĞLU , B.Sc.(ITU)

Date of Submission : February 03, 1992

Date of Approval : February 21, 1992

Supervisor : Assoc.Prof.Dr. M. Fevzi ÜNAL

Member : Prof.Dr. R. Alsan MERİÇ

Member : Assoc.Prof.Dr. M. Adil YÜKSELEN

FEBRUARY 1992

ACKNOWLEDGEMENTS

My sincere thanks must first go to my long–term supervisor Assoc. Prof. M. Fevzi ÜNAL for his priceless guidence and help throughout the study.

This work was supported by NATO. We greatfully acknowledge the NATO Collaborative Research Grant CRG 890427. Research Fellowship provided by the Faculty of Aeronautics & Astronautics is also greatfully acknowledged.

My appreciations must then go to my dear friends and colleagues at ITU especilly to Mr. Alpay Yılmaz, Mr. H.İbrahim Keser and A. Ruhşen Çete for sharing their experiences and knowledge.

I would also like to thank my dear friend H.Barbaros for his help in printing my thesis.

Finally, I am thankful to my family for everything they have done for me.

CONTENTS

CHAPTER 4.

LIST OF SYMBOLS

C_D	:	drag coefficient
C_F	:	force coefficient
C_L	:	lift coefficient
D	:	cylinder diameter
f	:	vortex shedding frequency
F_v	:	vortex force
L	:	length of splitter plate measured from the base of the cylinder
L_p	:	length of splitter plate measured from the center of the cylinder
MY	:	number of grid points in $-y$ direction
NX	:	number of grid points in $-x$ direction
R	:	cylinder radius
p	:	pressure
Re	:	Reynolds number
St	:	Strouhal number
T	:	dimensionless time
u, v	:	velocity components in $-x$ and $-y$ directions respectively
U_∞	:	free-stream velocity
$\vec{U}$	:	velocity vector
z	:	physical plane
α	:	step size in angular direction in intermediate (circular) plane
β	:	first moment of vorticity
Δt	:	integration time step
Δy_{wall}	:	distance between wall and wall+1 meshes in $-y$ direction in computation plane
Δx	:	distance between successive two meshes in $-x$ direction in computation plane

Γ	:	circulation
μ	:	dynamic viscosity
ν	:	kinematic viscosity
ω	:	vorticity in $--z$ direction
ψ	:	stream function
ρ	:	density
ξ	:	computation plane (semi-infinite plane)
ζ	:	intermediate plane (plain cylinder plane)

SUMMARY

In this study, a passive control of wake formed from a circular cylinder has been investigated. The passive control is achieved using a splitter plate attached to the base of circular cylinder.

Vortex–in–Cell (VIC) method forms the basis of the numerical method. The Navier–Stokes equations in two dimensions are solved using the operator–splitting technique: Convection and diffusion are treated separately. When modelling convection, a mixed Eulerian–Lagrangian scheme is used. The key to this hybrid scheme is to by–pass the Biot–Savart law and use sequentially the Lagrangian frame to track the vortices and the Eulerian frame to calculate the velocity field through the use of the Poisson equation for the stream function. The diffusion, on the other hand, is calculated on mesh using the Finite Difference Technique.

The effectiveness of splitter plates in reducing the drag of circular cylinders was examined and it was found, for example, that a splitter plate with a length 1.5 times the cross flow width of a cylinder could reduce the drag by as much as a third. In accord with experimental studies, the formation length of vortex experienced changes with varying plate length and the Strouhal number reached to a minimum value at about $L/D = 1.5$. Additionally, a secondary vortex formation from the tip of the plate emerges to be a part of a possible mechanism responsible for the experimentally observed variations in flow characterictics such as the Strouhal number.

ÖZET

DAİRESEL SİLİNDİRDEN OLUŞAN İZ AKIŞININ AYIRICI LEVHA İLE PASİF KONTROLU: VİSKOZ VIC BENZEŞİMİ

Küt cisimler etrafındaki akış ve bu akışın oluşturduğu iz bölgesi birçok mühendislik dalının ilgi alanına girmektedir. Yüksek binaların, köprülerin rüzgar etkisi de göz önüne alınarak tasarımı veya ısı değiştirici tüp demetlerinin tasarımı ve daha pek çok benzer mühendislik uygulamaları iz akışının ne denli önemli olduğunu göstermektedir. Küt cisimler arasında, geniş bir uygulama alanı olması nedeniyle dairesel silindir özel bir öneme sahiptir. Araştırma çalışmaları arasında da, dairesel silindirin sıklıkla ve uzun bir zamandır ele alındığı görülmektedir. Ancak, Strohal'ın 1870 lerde yaptığı gözlem ve çalışmalardan itibaren günümüze kadar yapılan birçok deneysel ve teorik çalışmalara rağmen, dairesel silindir etrafındaki akış birçok araştırıcı için cazibesini korumaktadır.

Dairesel silindir gibi küt bir cismin maruz kaldığı yükleme hali iz bölgesinde yer alan olaylarla yakından ilgilidir. Sınır tabakaların, cismin alt ve üst yüzeyleri üzerinde gelişimlerini takiben ayrılmaları ile ortaya çıkan girdap olarak adlandırdığımız akış yapısı sonuçta aşağı akım bölgesine taşınarak Karman Vorteks Caddesi olarak anılan yapıyı oluşturur. Sınır tabakaların alt ve üst yüzeylerden aralarında belirli bir faz farkı ile ayrılmaları cismin üzerine gelen kuvvetlerin de periyodik bir karakterde olmasını sağlar. Örneğin, taşıma katsayısı, sıfır ortalama etrafında ve vortex oluşum frekansında bir çalkantı gösterir. Sürükleme kuvveti de belirli bir ortalama etrafında girdap oluşum frekansının iki katında bir çalkantı içermektedir. Bu durumda yeteri kadar büyük genlikte ve uygun bir frekansta tekrarlı yükleme halinin izin oluşumundan sorumlu olan veya o iz akışı ile etkileşimde bulunan bir cismin uzerinde tahrip edici olacağı aşikardir. Dolayısı ile, şu veya bu şekilde, girdap oluşumunun kontrol altına alınması veya mümkünse tamamen ortadan kaldırılması, sözü edilen tahripkar durumdan uzaklaşmak için önemli olmaktadır.

Vorteks oluşumunun kontrolu aktif veya pasif denebilecek yöntemlerle sağlanabilmektedir. Aktif kontrolde doğrudan akış içinden alınan bir sinyalin işlenerek bu işlenmiş sinyal uyarınca iz akışına müdahalede bulunulması söz

konusudur. Örneğin, Williams ve Zhao (1989) girdap caddesine yerleştirdikleri bir sıcak tel anemometresinden aldıkları sinyali işleyip, bunu tünel duvarına yerleştirilmiş bir hoparlörü çalıştırmada kullanarak bir kontrol çevrimi oluşturmuştur. Sinyal uygun şekilde bir tür işleme tabii tutulduğunda, hoparlörden yayılan ses dalgaları girdap oluşumunu tamamıyla ortadan kaldırmaktadır. İz akışının pasif kontrolunde ise, akışa yapılan müdahalenin karakteri farklıdır. Müdahale, örneğin akış alanına küt cismin tabanından akışkan üflenmesi veya emilmesi, cismin ısıtılması veya soğutulması, akış alanına ikinci bir cismin yerleştirilmesi v.b. şeklinde olmaktadır. Buradaki çalişmada, pasif kontrol dairesel silindirin tabanına serbest akıma paralel olacak şekilde bir levha monte edilerek sağlanmaktadır.

Literatürde, ayırıcı levhanın küt cisim iz akışı üzerine etkisini araştıran çalışmalara çok nadir olarak rastlanmaktadır. Bu çalışmalardan en önemlisi Roshko (1954), Apelt, West & Sczewczyk (1973), Gerard (1966) ve Bearman (1965) olarak sayılabilir. Rastlanan tek sayısal çalışma ise Kawaı (1990) tarafından yapılmiştir. Bu çalışmada dairesel silindiri temsil eden hız potansiyeli, dairenin merkezine yerleştitilmiş bir duble ve serbest akımın hız potansiyellerinin toplamı şeklinde ifade edilmiş, ayırıcı levha ise bir dizi kaynakla temsil edilmiştir. Silindirin alt ve üst yüzeylerinden ayrımış sınır tabakaları temsil etmek üzere bırakılan potansiyel girdapların yörüngeleri Biot–Savart yöntemi ile bulunmuştur.

Deneysel çalışmalarda, ayırıcı levhanın etkin bir kontrol aracı olduğu, uygun levha boyunun sürükleme kuvvetinde önemli ölçüde azalma sağladığı ve Strouhal sayısının da belirli miktarda kontrol edilebildiği ortaya koyulmuştur. Ancak, halihazırda, bu kontrolun nasıl bir fiziksel mekanizma ile sağlandığı açık değildir. Fiziksel anlayışımızı geliştirmek için, yeni deneysel çalişmalara ve güvenilir yöntemlerle sayısal çalışmalara ihtiyaç vardır. Burada yapılan sayısal çalışma, kısmen de olsa bu ihtiyaca cevap vermeyi amaçlamaktadır. Sayısal çalışmanın esasını, viskoz ayrık girdap yöntemi oluşturmaktadır. Viskoz olmayan "Lagrange"sal ayrık girdap yöntemindeki Biot–Savart yasasının kullanılması yerine, bu yöntemde girdap konumlarındaki hizlar, akım fonsiyonu için Poisson Denklemi çözülerek bulunmakta ve bu hızlardan yararlanılarak girdaplar yeni konumlarına ilerletilmektedir. Yani Euler–Lagrange yaklaşımlarının birlikte kullanıldığı melez bir yöntem kullanılmaktadır.

Yöntem iki boyutlu Navier–Stokes denklemlerinden elde edilen Girdaplılığın Taşınımı Denklemini'ni (GTD) (Vorticity Transport Equation) çözer.

İki boyutta Navier–Stokes denklemleri;

$$\frac{\partial u}{\partial t}+u\frac{\partial u}{\partial x}+u\frac{\partial u}{\partial y}=-\frac{1}{\rho}\frac{\partial p}{\partial x}+\nu\left[\frac{\partial^2 u}{\partial x^2}+\frac{\partial^2 u}{\partial y^2}\right] \tag{1.a}$$

$$\frac{\partial v}{\partial t}+u\frac{\partial v}{\partial x}+v\frac{\partial v}{\partial y}=-\frac{1}{\rho}\frac{\partial p}{\partial y}+\nu\left[\frac{\partial^2 v}{\partial x^2}+\frac{\partial^2 v}{\partial y^2}\right] \tag{1.b}$$

şeklindedir. Bu denklemlerin çapraz türevleri alınır ve basınçlar yok edilirse GTD elde edilir:

$$\frac{\partial \omega}{\partial t}+(\vec{U}.\nabla)\omega=\nu\nabla^2\omega \tag{2}$$

Burada ω z yönündeki girdaplılığı ifade etmektedir. Bu denklem Difüzyon (3) ve viskoz olmayan Taşınım (4) olarak iki parçaya ayrılabilir

$$\frac{\partial \omega}{\partial t}=\nu\nabla^2\omega \tag{3}$$

$$\frac{\partial \omega}{\partial t}=-(\vec{U}.\nabla)\omega \tag{4}$$

ve ardışık olarak çözülebilir. Lineer olmayan yapıdaki taşınım terimleri esas denklemden ayrılarak çözüm kolaylığı sağlanmaktadır. Ayrıca yöntemin, difüzyon ve taşınım için değişik çözüm teknikleri ve değişik yaklaşımlar kullanılmasına izin vermesi bir diğer avantajdır. Bu çalışmada tercih edilen, difüzyonun Eulerian, taşınımın ise Eulerian–Lagrangian, melez yaklaşımla çözümüdür.

Yöntemin akım alanına uygulanabilmesi için cisim etrafında bir ağ (grid) üretmek gereklidir. Çözümler dikdörtgensel yarı sonsuz düzlemde yapılmıştır. Bu yüzden de yarı sonsuz düzlem ile ayırıcı levhalı silindir düzlemleri arasında bir dönüşüme ihtiyaç vardır. Bu Jukowski dönüşümü ile aşağıdaki şekilde elde edilmiştir. Burada z fiziksel düzlemi, ζ da (dönüşüm) hesaplama düzlemini göstermektedir.

$$z=F\pm\sqrt{F^2-1} \tag{5}$$

ki burada

$$F=\frac{(1+L)^2}{8L}\left(\zeta+\frac{1}{\zeta}\right) \tag{5.a}$$

Bu ağ üzerinde ilk önce akım fonksiyonu değerleri Poisson denklemine göre hesaplanır. Poisson denklemi, girdaplılığın

$$\omega=\frac{\partial v}{\partial x}-\frac{\partial u}{\partial y} \tag{6.a}$$

ve akım fonksiyonunun

$$u = \frac{\partial \psi}{\partial y} \qquad\qquad v = -\frac{\partial \psi}{\partial x} \tag{6.b}$$

olacak şekilde tanımlanması ile, süreklilik denkleminden

$$\nabla^2 \psi = -\omega \tag{7}$$

şeklinde elde edilir. Bu denklem iteratif veya doğrudan metodlarla çözülebilir. Bu çalışmada eliptik yapıdaki Poisson denkleminin çözümü için ÇFD (Çabuk Transform Dönüşümü) kullanılmıştır. Her bir ağ noktasındaki akım fonksiyonu değerleri elde edildikten sonra, katı cidarda kaymama sınır şartından uygun girdaplılık değerleri.

$$\omega_w = -\frac{2(\psi_{w+1} - \psi_w)}{h^2} \tag{8}$$

şeklinde elde edilir. Burada, h cidarla cidara yakı ağ noktası arasındaki uzaklık, ψ_w ve ψ_{w+1} ise bu noktalara sırası ile tekabül eden akım fonksiyonu değerleridir. Taşınım için 1950'lerin başında ortaya atılan ve zamanla gelişip çok popüler olan Hücre içinde Girdap (Vortex–in–Cell) tekniği kullanılmaktadır . Bu teknikte her bir girdap, içinde bulunduğu hücrenin köşeleriyle etkileşim halindedir. Poisson ve difüzyon denklemlerinin çözümünde kullanılan ağ noktalarındaki girdaplılık değerleri girdapların hücre içindeki konumuna göre alan interpolasyonuyla köşelere dağıtılır. Böylece, Poisson denkleminin (7) sağ tarafı oluşturulmuş olur ve bu denklemin çözümü ile ağ noktası hızları belirlenir. Bu hızlardan geriye interpolasyonla girdaplar üzerine indüklenen hızlara geçilir ve taşınım sağlanır.

Bu teknikle, Biot–Savart indüksiyon metodunda olduğu gibi her bir girdap üzerindeki hız diğer girdapların etkisiyle hesaplanmaz. Bu yüzden merkezi işlem zamanı bir hayli kısalmaktadır. Biot–Savart indüksiyonu ile gereken ortalama işlem sayısı N^2 (N Vorteks sayısı) iken, bu yöntemde $M \log_2 M$ (M ağ nokta sayısı)dir.

Yöntem uygulanırken, sonuçların ağ yapısından bağımsız olarak belirlenmesi için, ağ yapısı için parametrik bir çalışma yapılmıştır. Hesaplama düzleminde, fiziksel düzlemdeki cisim cidarına tekabül eden dikdörtgensel düzlemin alt kenarı boyunca sabit aralıklı bir ağ üretilmiştir. Bu, Poisson Denklemi çözümünde ÇFD kullanılması nedeni ile ortaya çıkan bir zorunluluk olmaktadır. Diğer taraftan, ağın cidara dik yöndeki yapısı belirlenirken, sınır tabaka içinde yeteri kadar ağ noktası kalması, ağın en dış sınırının ise yeteri kadar uzun hesaplama zamanına imkan tanıması amaçlanmıştır. Bu nedenle, ağ cidara dik yönde genişleyen bir karakterdedir. Cidardan uzaklaşırken, hücre büyüklüğü artımının yavaş olmasına dikkat edilmiştir. Ayrıca seçilen Reynolds sayısına, hesaplama düzleminden fiziksel düzleme geçişte dönüşüm modülünün en küçük değerine ve en küçük hücre boyutuna bağlı olarak, en büyük integrasyon zaman aralığı kararsızlık oluşturmayacak şekilde belirlenmiştir. Sonuçta, fiziksel düzlemde, cidara hemen komşu hücrenin cidara dik doğrultudaki uzunluğu, yarıçapa oranla 0.05 dir; en büyüğü ise 628 olmaktadır. Fiziksel düzlemde ağ cisim merkezinden 1308 yarıçap aşağılara kadar uzanmaktadır. Yarıçap ve serbest akım hızına göre boyutsuzlaştırılmış integrasyon zaman aralığı ise 0.005 dir. Bu zaman aralığı difüzyonda kararsızlık oluşturmayacak şekilde belirlenen en büyük zaman aralığından oldukça büyüktür. Böylesi büyük bir zaman aralığı hesaplama imkanlarının yetersiz oluşu nedeni ile seçilmiştir.

Ayırıcı levhanın iz karakteristiklerine etkisi altı değişik levha boyu ele alınarak incelenmiştir. Bunlar, silindir çapı ile boyutsuzlaştırılmış haliyle $L/D = 0.25, 0.5, 1.0, 1.5, 2$ ve 2.5 dir. $L/D = 0$, yani ayırıcı levhasız silindir referans hali olmaktadır. Bu hal için literatürde deneysel, sayısal çok sayıda çalışma bulunmaktadır ve dolayısı ile hakkında nisbeten en çok bilgi sahibi olunan haldir. Bu nedenle de yukarıda belirtilen, ağ yapısı için parametrik çalışmada yol gösterici olmuştur. Çalışmada kullanılan viskoz kod, akış yapısına başarı ile benzeşim sağlamakla kalmayıp, sürükleme ve taşıma katsayıları (C_D, C_L) ve Strouhal sayısı (St) gibi büyüklüklerin deneysel sonuçlara uygun olarak bulunmasını sağlamkatadır.

Ayırıcı levha bulunması halinde de sürükleme katsayısı C_D ile Strouhal sayısı (St) ayırıcı levha boyuna göre deneysel çalışmalarda belirlenen tarzda değişmektedir. Çapın 1.5 katı uzunluğundaki ayırıcı levhanın silindirin maruz kaldığı sürükleme kuvvetini levhasız hale göre %30 a yakın bir oranda düşürmesi deneysel sonuçlarla uyum içindedir. Strouhal sayısının artan levha boyu ile önce azalması sonra ise artması da deneylerle uyum içindedir. Ancak, azalma oranı bu çalışmada deneysel çalışmalara göre oldukça büyük olarak ortaya çıkmaktadır. Strouhal sayısının azalma oranındaki bu uyumsuzluk halihazırda araştırılmaktadır. Global büyüklüklerdeki bu değişimler, elbette ki silindirin alt ve üst yüzeylerinden gelişen sınır tabakaların ayrılmalarını takiben girdap oluşumu ile son bulan gelişimlerinde ayırıcı levha boyuna göre gözlenen değişimlerle yakından ilişkilidir. Ayırıcı levha boyu arttıkça girdap oluşum uzaklığı artmakta, diğer bir deyişle girdabın tam gelişmiş hali ile ortaya çıkması silindirden gitgide daha uzak akımaltı bölgelerine kadar ertelenmektedir. Buna paralel olarak, alt ve üst taraflardan ayrılan sınır tabakalar arasındaki etkileşim ayırıcı levha boyu arttıkça gitgide artan oranda sınırlanmaktadır. Ancak, burada ilginç olarak ikinci bir tür etkileşim ortaya çıkmaktadır; ayırıcı levha ucunda oluşan ikincil bir girdap olşumu gözlenmekte ve bu girdap büyük ölçekteki birincil girdap ile etkileşimde bulunmaktadır. Bu etkileşimin, örneğin Strouhal sayısı gibi bir büyüklüğün levha boyuyla değişiminde ne gibi bir etkisi olduğunu belirlerken, girdap oluşum uzaklığı ve tam gelişmiş girdabın şiddetindeki değişikliklerin de göz önüne alınması gereklidir. Vorteks oluşum uzaklığı artan levha uzunluğu ile artmakla birlikte bu artım ilelebet devam etmemekte, belirli bir levha boyundan sonra artık bir artım olmamaktadır. Dolayısı ile de levha ucu girdabının oluşumu ile birincil girdap oluşumu arasında levha boyuna bağlı olarak değişen faz farklılıkları gözlenmektedir. Örneğin, girdap oluşumunun ancak levha ucuna kadar ertelendiği levha boylarında, pozitif işaretli bir birincil girdap, negatif işaretli bir uç girdabı ile birlikte oluşurken, girdap oluşumunun levha ucundan geriye düştüğü uzun levha boylarında aynı işaretli birincil ve uç girdaplar birlikte gözükmektedir. Birincil ve ikincil girdapların etkileşimi sonucu ortaya çıkan büyük ölçekteki nihai girdabın, bu durumda, değişen levha boyuna göre farklı şiddetlerde ortaya çıkacağı aşikardır. Daha büyük şiddetteki nihai girdabın daha küçük şiddettekine göre daha büyük bir Strouhal sayısına yol açacağı şeklindeki genel kanı dikkate alınırsa, Strouhal sayısının artan levha boyu ile önce azalması sonra da artmasında birincil girdabın uç girdabı ile etkileşimi mekanizmasının belirleyici olduğu ileri sürülebilir. Bu iddianın doğruluğu, Imperial College Havacılık Bölümü su kanalındaki akım görünürlüğü deneyleri ile sınanacaktır.

CHAPTER 1

MECHANISM OF VORTEX FORMATION

1.1 Vortex Shedding from a Circular Cylinder

In the case of fluid motions for which the measured pressure distribution nearly agrees with the perfect-fluid theory, such as the flow past an airfoil, the influence of viscosity at high Reynolds numbers is confined to a very thin layer in the immediate neighbourhood of the solid wall. If the condition of no-slip were not be satisfied in the case of a real fluid there would be no appreciable difference between the field of the flow of the real fluid as compared with that of a perfect fluid. The fact that at the wall fluid adheres to it means, however, that frictional forces retard the motion of the fluid in a thin layer near the wall. In that thin layer the velocity of the fluid increases from zero at the wall (no-slip) to its full value which corresponds to external frictionless flow. The layer under consideration is called *boundary-layer* [1]. The decelerated fluid particles in the boundary-layer do not, in all cases, remain in the thin layer which adheres to the body along the whole wetted length of the wall. In some cases the boundary-layer thickness increases considerably in the downstream direction and the flow in the boundary-layer becomes reversed. This causes the decelerated fluid particles to be forced outwards, which means that the boundary-layer is separated from the wall. This phenomenon is called *boundary-layer separation* which is always associated with the formation of vortices and with large energy losses in the wake of the body. It occurs primarily near blunt bodies, such as circular cylinders and spheres.

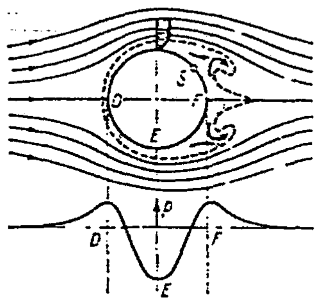

Figure 1.1 Boundary–layer separation and vortex formation on a circular cylinder,S= Separation point [1]

The phenomen of boundary layer separation is illustrated in Fig [1.1] : A fluid particle is accelerated on the upstream half from D to E and decelerated from E to F. Hence the pressure decreases from D to E and increases from E to F. Owing to the large friction forces in the thin boundary-layer such a particle comsumes most of its kinetic energy on the path D to E , and the reminder is not enough to surmount the pressure hill from E to F. So this particle cannot move far into the region of increasing pressure between E and F, and its motion is, extremely, arrested. The external pressure causes it then to move in the opposite direction. This is what is called as boundary-layer separation for a circular cylinder. For a circular cylinder in a uniform flow with velocity U_∞, velocity around it is;

$$U(x) = 2U_\infty \sin \frac{x}{R} \tag{1.1}$$

where x denotes the arc measured from front stagnation point and R is the radius of the cylinder. Then the time when separation occurs is [1];

$$t_s = \frac{R/U_\infty}{2(1+\frac{4}{3\pi})} \tag{1.2}$$

and the distance covered until separation is

$$\delta_s = 0.351R \tag{1.3}$$

This separation highly dependent on Reynolds number. Maximum distance from the front stagnation point at which the boundary-layer remains attached is dependent on how energetic the fluid is in the close neighbourhood of the surface. To illustrate, flow at high Reynolds numbers shows a longer distance of separation position than one at low Reynolds numbers does. Figure[1.2]

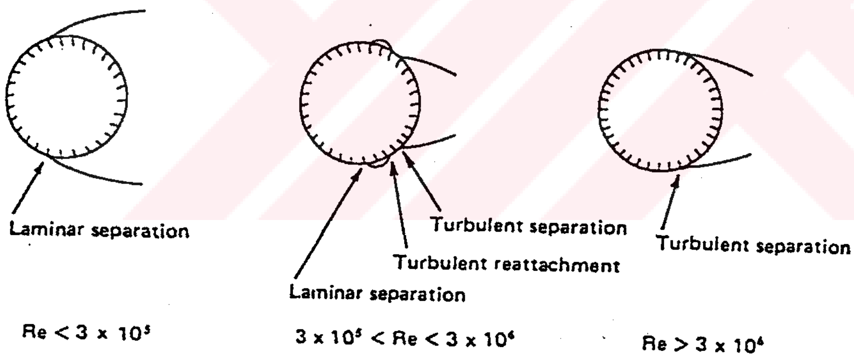

Figure 1.2 Separation positions for various Reynolds number ranges [2]

This brings narrower wake at high Reynolds numbers and it can be shown from the conservation of linear momentum that this narrower wake results in lower form drag. These features can be clearly observed from the Figures [1.3],[1.4]

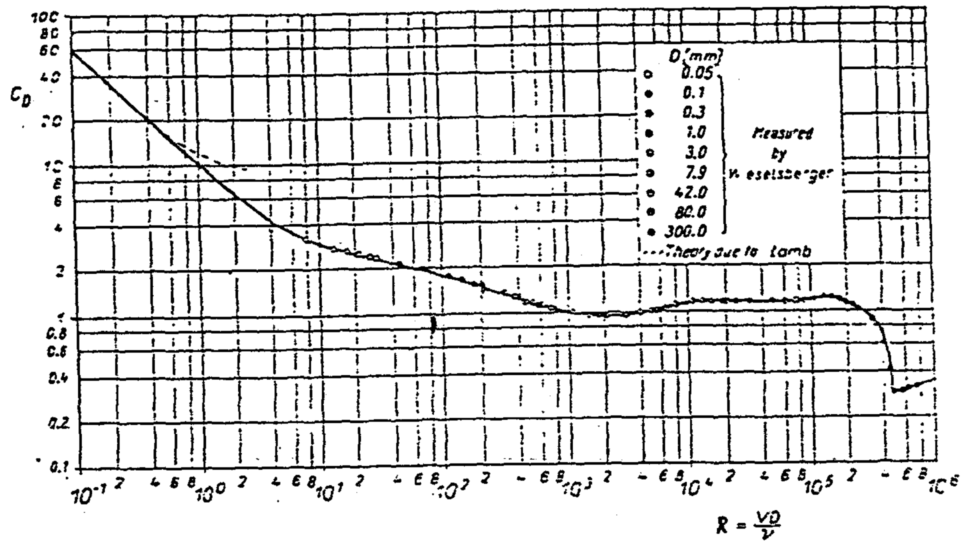

Figure 1.3 Drag coefficient for circular cylinders as a function of the Reynolds number[1]

Periodic vortex formation following the separation of boundary layers from upper and lower sides of a 2–D bluff body builts a structure downstream of the body with particles moving alternately clockwise and counterclockwise directions. This structure is known as Karman Street after his work on wake mechanism [3]. Blevins [4] gives the following description for the regimes of flow around circular cylinders also summarized in Fig [1.4]: At very low Reynolds numbers (i.e. $Re < 5$) based on the cylinder diameter, the flow is unseparated. For a higher Reynolds number range a fixed pair of Föppl vortices are observed close behind the cylinder. As Re is further increased, these vortices elongate and break away and thus form a periodic wake with staggered vortex street. Re of approximately 150 marks the point up to which the vortex street is fully laminar. At a Re of 300, the street is turbulent and degenerates into fully turbulent flow beyond approximately 50 diameters downstream of the cylinder. The Re range of 300 to approximately 3×10^5 has been called the subcritical range, because it occurs prior to the onset of the turbulent boundary layer at a Re of approximately 3×10^5. The shedding occurs at a well defined frequency in the subcritical Re range. However, at the transition Re, the flow separation point moves backwards, the vortex shedding is disorganised and the cylinder drag drops sharply [see also Fig 1.3]. At higher supercritical Re ranges the vortex street re–establishes itself.

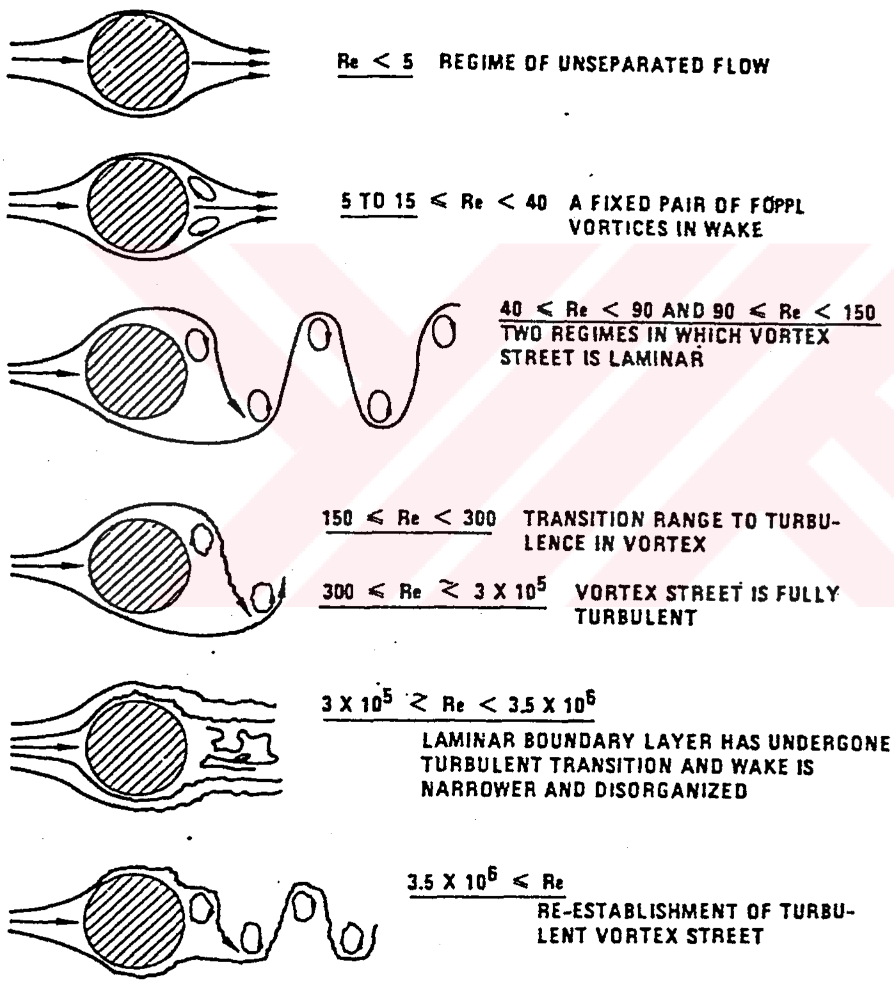

Figure 1.4 Regimes of fluid flow across circular cylinders [4]

Since the Strouhal's experiment in the late 19th century, a wake of a circular cylinder has been subject to formal investigations. Strouhal found that the frequency of vortex shedding generated by a circular cylinder is proportional to the wind speed divided by cylinder radius that is $f \sim U/D$. Following him, Rayleigh defined a non-dimensional quantity which is known as the Strouhal number. The Strouhal number for circular cylinder is shown in Fig [1.5].

$$St = \frac{fD}{U} \tag{1.4}$$

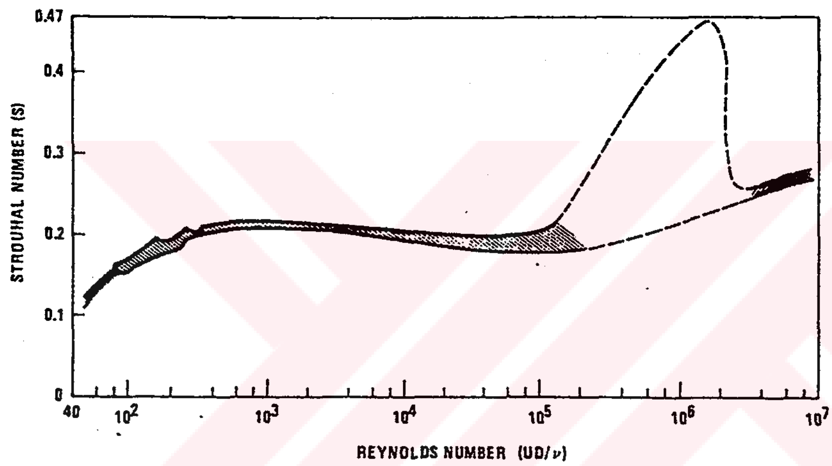

Figure 1.5 The Strouhal–Reynolds numbers relationship for circular cylinders [4]

After that, Roshko [5] defined such a universal number that the number is not dependent on the thickness of the body responsible for the wake but the distance between the boundary layers (wake width) separated from the body. This definition constitutes the idea in the article of Abernathy & Kronauer [6] " given two parallel vortex sheets separated by some initial distance; is it necessary to have a solid body between them in order to form a vortex street? The answer is definitely no." In their work, they consider two infinite vortex sheets, initially a fixed distance,h, apart, in an inviscid incompresibble fluid, and calculate the non–linear interaction of these sheets for various ratios of h to wavelength, a, of the initial disturbance. The nonlinear interaction give rise to a vortex street formation and the value of h/a does not alter the general pattern of the vortex street but rather influences the details of the interactions. In contrast to this study cocentrated to the vortex street region, Gerrard [7] draws the attention to the events taking place in the region of flow just behind a bluff body. In a physical discussion of the mechanics of the formation region, he introduces a relationship among the size of the formation region, the strength of the vortices and the frequency of vortex shedding.

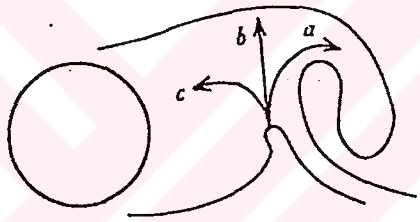

Figure 1.6 Filament line sketch of the formation region. Arrows showing reverse flow (c) and entrainment (a) and (b) [7]

The end of the formation region is defined as the point on the wake axis, closest to the cylinder at which a hot–wire signal shows a sudden reduction of the low–frequency irregularities always observed in the formation region [8]. This definition agrees well with that based on the location of the maximum intensity of longitudinal velocity fluctuations at first harmonic frequency on the wake axis [9]. The position at which the streamwise velocity fluctuations along a line parallel to the wake centerline reach a maximum can also be taken as the end of the formation region [10]. All of these imply that the end of the formation region is where fluid from outside the wake first crosses the wake axis. It is this definition which is employed in the study herein. Going back to the definition of vortex formation presented by Gerrard, we see that an entrainment process is proposed to have a determining role in the vortex shedding: Figure [1.6] shows the instant when irrotational fluid is begining to cross the wake axis. At later times, this fluids follows the paths indicated by arrows: It is partly entrained by the growing vortex and partly by the shear layer upstream of the vortex. Some of it also finds its way into the interior of the formation region. The entrainment of fluid bearing vorticity from the other shear layer takes place periodically, and this periodic entrainment of fluid across the wake has a predominant influence in the vortex shedding. In other words, circulation supply to the growing vortex is cut by the circulation of opposite sign drawn accross the wake. Another explanation for the mechanism of vortex formation that is different but not contradicting the one given by Gerrard is due to Ünal & Rockwell [11]. According to them, it is the absolute instability of the separated boundary layers that gives way to the vortex formation.

An interesting feature of the vortex formation from a circular cylinder is the appearence of secondary vortices from the downstream face of the cylinder. The experimental work of Bouard & Coutanceau [12] shows that, at Reynolds numbers greater than 300 there appear small eddies near the wall of an impulsively started circular cylinder. At an earlier study, Thoman & Szewczyk [13] also report generation of such eddies having circulation of opposite sign with respect to the large scale vortex. The numerical work of Ta Phouc Loc [14], based upon vorticity–stream function formulation analysis the mechanism of the creation of secondary vortices behind an impulsively started circular cylinder, in the Reynolds number range 300-3000. However, all of these studies are limited to the early stages of development of flow behind the cylinder. In a recent study Braza et. al. [15] numerically study the near wake of a circular cylinder and disclose the details of the generation of the secondary, counter rotating vortices and their interaction with the main vortices. Interestingly, they show this generation–interaction process as a cause to the relative constancy of the Strouhal number in a wide Reynolds number range beyond Re=200. From the above mentioned point of view put forward by Gerrard, less coherent vortex resulting from the interaction of the small scale, counter rotating vortex with the main one implies a longer formation length and a smaller Strouhal number in comparison with the case that would have appeared if there were no secondary vortex formation. Then, it becomes an unresolved issue if such a secondary vortex also exists in the case of circular cylinder with a splitter plate attached to its end and to what extend this generation plays a role in controlling the wake flow characterictics such as the Strouhal number of vortex shedding. Herein, the primary concern is to numerically disclose the details of the vortex formation process to give a physical explanation to the experimentally observed variations in the wake characterictics of a circular cylinder with the splitter plate.

1.2 Control of Wake from a Circular Cylinder and Effects of Splitter Plate

The unsteady condition of a wake from a bluff body such as a circular cylinder gives ways to undesirable high mean drag as well as high fluctuating values in the lift force. However, many studies show that in an active or passive way bluff body flows can have quite desirable characterictics.

Understanding the physics of vortex shedding is central in proposing an effective means of controlling the bluff body wake characteristics. In this context, experimental studies on especially the near wake region of bluff bodies are relevant. Gerrard [16] shows that the oscillating properties of the flow past a circular cylinder in the Reynolds number range 2×10^3 to 5×10^4 are highly susceptible to small disturbances. If the level of disturbance is low there is a large increase in fluctuating lift coefficient and the fluctuating velocity at the side of the cylinder as the Reynolds number increases from 2×10^3 to about 5×10^4. If the flow subjected to acoustic radiation at the frequency of the transition waves which precede the turbulent flow in the shear layers shed from the cylinder, the range of Reynolds number over which the quantities show this large increase is shifted to lower Reynolds number. Similarly,for Reynolds number at the order of 10^4 , Peterka & Richardson [17] show that, with a sound field having its frequency matched sufficiently closely to that of the transition waves the instability in the shear layer is enhanced and the vortex formation length is reduced. However, the vortex street frequency is very weakly affected. In summary, the sound radiation at an appropriate frequency can alter the flow characteristics of a circular cylinder wake such as the formation length at least in a limited range of Reynolds numbers. More recently, for Reynolds number

400, Williams & Zhao [18] showed that the flow around a circular cylinder can be actively controlled by an acoustic feedback of signals taken from hot–wires in the wake of the cylinder.

Another way of controlling the characteristics of wakes from a circular cylinder is to use end–plates [19]. Gerich & Eckelmann show that, if the distance of two end–plates is appropriate the upper limit of the laminar range of vortex street wake is extended from 160 to 250. Control of bluff body wake is also achieved using a modified trailing–end. Greenway & Wood [20], based on the flow visualization technique, demonstrate that a bevelled trailing–edge provides an asymmetric circulation distribution in the vortex formation region and thus suppress the vortex–excited vibration of the flat plate responsible for the wake.

Passive control of wake from a circular cylinder is also achieved by a proper placement of a second, much smaller cylinder in the near wake of the main cylinder (Strykowsky & Sreenivosan [21], Yılmaz [22]). Strykowsky & Sreenivosan show that this secondary cylinder can alter the vortex shedding and suppress it altogether over a limited range of Reynolds numbers. Since the early experiment of Roshko [23], passive control of wake by means of a splitter plate placed downstream of a cylinder in different arrangements has been studied by many authors. Ünal & Rockwell [24], Smith & Karamcheti [25] show that a splitter plate placed at a distance downstream of a circular cylinder is a possible way of controlling the bluff body instabilities. Ünal & Rockwell found out that when the plate is located downstream of the initially formed vortex, effective control is possible when the near wake fluctuation level and mean base pressure of the corresponding free wake (without the splitter plate) are sufficiently small. The wake impinging upon the splitter plate creates unsteady pressure fluctuations there in turn, these pressure fluctuations induce an upstream influence at the sensitive region near separation points of the boundary layers. This phenomenon occurs between separation and impingement simultaneously i.e. they are not of consequence of each other. They form a close loop. If the slitter plate is placed far enough downstream to allow for the evolution of the vortex street the near wake of a bluff body has a high degree of self–control and therefore is insensitive such an upstream influence.

Other ways of the controlling the wake of a bluff body is to steadily supply a small amount of fluid into the base region (base–bleed) [10] or to employ a splitter plate attached to the base of the body [26] ,[27] . Both of these methods have been proven to be an effective means of controlling the near–wake characteristics, such as the Strouhal number of vortex shedding, the formation length of vortices, etc.

CHAPTER 2

AN OVERVIEW OF NUMERICAL APPROACHES WITH VORTICES

Helmholtz, who gave one of the most important contributions to fluid mechanics, showed that in an inviscid fluid vortex lines remain continually composed of the same fluid elements and flows with vorticity can be modelled with vortices of appropriate circulation and infinitely small cross section. This brings forth the discretization of the compact region of vorticity into an assembly of vortices embedded in an otherwise potential flow. Such a discretization of vorticity field with point vortices leads to the Lagrangian approach for calculating the evolution of the vorticity field: Point vortices are introduced into the flow field and traced numerically by applying the Biot–Savart law of induction. Being grid–free, this method eliminates the problem of numerically generated viscosity. However, there are difficulties associated with the Biot–Savart approach even for two–dimensional flow simulations with point vortices. First, the point vortices are singularities, and therefore, create large velocities in their neighbourhood. This causes instabilities and physically impossible sheet crossings along and near the edge of the sheet represented with an array of discrete vortices. The second difficulty is that the number of operations required for the velocity field calculation is proportional to N^2 where N is the number of vortices. Therefore the computation time for complex flows with high number of vortices becomes too long to be practicle. To cope with these difficulties, various smoothing techniques such as amalgamation and rediscretization of vortices and hybrid methods making the use of Eulerian–Lagrangian approaches are used. For a summary of smoothing techniques, the reader may refer to a recent review by Sarpkaya [28]. The key to the hybrid approach is to by–pass the Biot–Savart law and to obtain the velocity field as a solution of the Poisson's equation for the stream–function across the mesh and consequently advance the vortices to their new positions using a Lagrangian approach. The basic advantage of VIC technique is that the number of velocity calculations does not increase as N^2 as in Biot–Savart approach. Poisson solvers require in the order of $Mlog_2M$ operations where M is the number of grid points. Therefore the VIC technique enables one to track a larger number of vortices (several thousand) compared with several hundred with the Biot–Savart method. However in some cases the time saved may be disappointingly small because of the Eulerian step overhead. An additional advantage gained through the use of VIC tecnique is the desingularization of the velocity field by smearing the vorticity over a cell area.

2.1 Lagrangian Discrete Vortex Method

In early studies of bluff body wakes using Lagrangian Discrete Vortex Method, the primary task was to find out the conditions for which a stable pattern of vortex street may exist. In these studies, the array of vortices were employed in representing the actual vortical structures encountered in the wake without taking the body responsible for the wake into consideration. Von Karman [3] took two parallel rows of vortices extending to infinity in both directions and found a ratio of the lateral spacing between two rows to longitudinal spacing between two consecutive vortices in the same row at which the vortex street remained stable. Abernathy & Kronauer [6] studied the non-linear interaction of two infinitely long vortex sheets, initially a fixed distance apart, in an inviscid and incompressible fluid.

More recent studies take into account the presence of bluff body and, by representing the separated boundary layers from the body by a row of potential vortices, aim to concentrate into the vortex formation mechanism taking place into the near wake region. Of course this time, in contrast to the examples of Karman and Abernauty & Kronauer, the potential vortices are not in an infinitely large flow field but limited with a solid boundary. Therefore, in an inviscid analysis, in order to satisfy the " no flow across the boundary " condition, the image vortices in the body should be accounted for. This brings forth a difficulty that not all the body geometries are suitable for the of image method. Only the geometries such as semi–infinite half plane or circular cylinder allow for finding analytical expressions for the location of image vortices. Pioneering works of Clements [29] and Sarpkaya & Schoaff [30] constitute two renown examples to the application of the Lagrangian Discrete Vortex Method with the image vortex technique to represent the body boundary. Clements transforms a semi–infinite half plate with a blunt trailing–end to a semi–infinite plane where the location of the image vortices are easily found. Whereas in the work of Sarpkaya & Schoaff, the image vortices are placed directly at their locations inside the circular cylinder. With the conformal mapping–image technique the flow around multiple bluff bodies can also be studied [31]. In These studies, vortices are succesively introduced into the flow field from upper and lower separation points and are tracked in time using the Biot–Savart law. Of course, in such inviscid simulations of the evolution of the separated boundary layers, it is not possible to predict the location of the flow separation unless the body has fixed separation points (e.g. flat plate, [29]). Therefore, a boundary layer solution to predict the separation points must be included to the inviscid analysis ([30], [32]). However, there are some inviscid approaches that allow for the prediction of the separation points based on the maximum velocity location on the boundary ([33], [22]). It should also be noted that many good studies ignore the variation of the separation points in harmony with the downstream periodicity altogether and keep them fixed at values close to the experimentally determined ones.

The discrete vortex methods with vortex and/or source based panel methods have been applied to single bluff bodies with simple geometries. The body surface is discretized into many segments (panels), and distribution of sources and/or vortices is assumed on the segments. By solving a system of linear equations at each time step for the unknown source and/or vortex, the strength of the vortex on each segment is determined so that the boundary condition is satisfied at the center of each segment (control point). Because neither the conformal mapping nor the superpositions of the image vortices are required, the vortex and/or source based panel methods can be applied to more complex body geometries. As to the introduction of the nascent vortices, vortex and/or source panel methods do not differ from the conformal mapping–image technique. In both of these, the nascent vortices are convected into the fluid at the separation points.

However, the vortex tracking method due to Spalart & Leonard [34] allows for introduction of many vortices all around the body surface into the flow field. In this method, the body is discretized into many wall points as in the panel method but the bound vortices are created around the body (not on the body surface) so that all the wall points are on a streamline. In view of the computational burden of the Lagrangian Discrete Vortex Method, it is obvious that the vortex tracking scheme requires powerful computers especially when the flow around multiple bodies are taken into consideration [35].

As mentioned above, the velocity induced by a point vortex is infinite at the center of point vortex, which is unrealistic for a real fluid. To avoid this, a Rankine vortex has been widely used in the vortex methods. The induced velocity by the Rankine vortex within the core is proportional to the radial distance from the center of the vortex and is the same as the velocity induced by the point vortex outside the core. Once the Rankine vortex concept is employed to remove the singularities due to point vortices one may as well allow for a time dependent core radius in order to simulate the viscous diffusion of circulation. However, it should be noted that, even though core expansion appears to simulate the viscous diffusion of the vortex this idealization violates Euler's equation and Helmholtz's laws. Nevertheless, the simulation of diffusion via core expansion has been used extensively. (e.g. [36] , [35])

A more precise way of simulating the viscous diffusion is the random walk method due to Chorin [37]. In this method, a random displacement with Gaussian probability distribution and zero mean and standart deviation $\sigma = \sqrt{2\Delta t/Re}$ is given to each computational element. Therefore the convection has a deterministic part given by the velocity induced at the vortex positions in addition to a random part named as the random walks. The vortex sheets diffuse perpendicular to the wall only and the sheets that penetrate the body are reflected back into the flow. However, Chorin [37] points out assesing the effect of interaction between the random and deterministic parts of the convection as a crucial problem associated with the random walk method : He states " we do not expect valid solutions at low Re ", and " at the other extreme, some difficulty may be expected at very high Re numbers. This is because the boundary layers formed by the algorithm are made up of a few bouncing vortices and are thus noisy; turbulence effects should therefore appear at too small a value of Re, as they do, for example, in noisy wind tunnels around rough bodies". Therefore, in order for the random walk method to work, one should increase the definition within the flow by using many discrete vortices which means more computational time. However at this stage, VIC method provides a useful tool in calculating the velocity field for large number of vortices.

2.2 Lagrangian-Eulerian Hybrid Discrete Vortex Method

In response to the need to reduce long CPU times involved in application of the Lagrangian Discrete Vortex methods using the Biot–Savart Law of Induction, Cloud–in–Cell (CIC) or Vortex–in–Cell (VIC) method [38] has become very popular among many researchers. The key to the execution of this grid dependent hybrid scheme is to by–pass the Biot–Savart law and use sequentially the Lagrangian frame to track the vortices and the Eulerian frame to calculate the velocity field through the use of Poisson's equation. This requires a fine–enough grid, the assumption that the vortices in a given cell temporarily become cell-shaped blobs with a prescribed vorticity distribution (often uniform), a vorticity allotment scheme which allocates vorticity to the surrounding mesh points (i.e. from the location of vortices to the nearest node points of the mesh), a numerical solution of Poisson's equation by a "fast Poisson solver" and an interpolation scheme which determines the velocities at the location of the original vortices from the node point values. The last step couples with a Lagrangian description of vortex convection, completing a cycle of the VIC scheme [28].

One obvious advantage of the VIC method is that it allows for calculation of viscous diffusion in various ways e.g. using the random walk method, employing a finite difference technique accross the grid. In the applications of the random walk technique, increasing the definition within the flow by introducing a large number of vortices around the surface becomes practical via the VIC technique. Stansby & Dixon [39] and Smith & Stansby, [40] applied the method in combination with the random walk method to a flow around circular cylinder up to Reynolds number of 10^4. The representation of the body is achieved using the vortex panel method.

Splitting the equations of flow into separate convection and diffusion equations, the idea central to all discrete vortex methods, gives way to alternative treatments of vorticity diffusion. Benson et. al. [41] applies a direct exact solution for the diffusion of vorticity at each time step followed by rediscretization onto a mesh of grid points to obtain the stream function solution of Poisson's equation for convection by the VIC method. The method is applied to low Reynolds number flows about circular cylinders with both steady and oscillating wakes, and the comparison with a finite element solution and with experimental results shows good agreement up to a Reynolds number of 200. The main drawback to such a diffusion algorithm is computational cost, although it does have the advantages over the random walk method, of higher accuracy at low Reynolds numbers. Another alternative treatment of diffusion of vorticity along with the VIC method for convection can be seen in the work of Vada et.al [42]. They account for dissipation in a primitive manner by reducing the strength of the vortices in time, and for viscous flow around a circular cylinder in the boundary layer near a wall, found an encouraging comparison with experimental data. Another direct solution of the diffusion of the point vortices involves extending the Eulerian part of the VIC scheme to calculate the diffusion on the mesh [43] . In contrast to vortex sheet creation to satisfy the no–slip boundary condition in the panel–based methods, herein, the vorticity at the solid surface is calculated by a finite difference approximation. Following the algorithm, the vorticity naturally diffuses from the surface, and to keep the number of point vortices at a reasonable amount, the newly formed vorticity, depending on its strength, is either amalgamated with the nearest point vortex to the mesh point, or, released as a separate vortex.

In this study, as in any other viscous discrete vortex method, the time splitting of the vorticity transport equation is used. While solving the convection part using the VIC method the diffusion of vorticity is solved directly on the mesh using finite difference technique. Detailed description of the solution procedure is in the following chapter.

CHAPTER 3

THEORY AND TECHNIQUE OF SOLUTION

3.1 Governing Equations

The fundamental equation of a flow for a Newtonian fluid is the equation derived from the balance of momentum,namely the Navier-Stokes equation. The balance of momentum for a fluid can be written as;

$$\rho \frac{D\vec{U}}{Dt} = \rho\vec{g} + \nabla.\vec{\sigma} \tag{3.1}$$

By taking $\vec{\sigma}$ in consideration according to the Stokes's postulates [44], for an incompressible and constant–viscosity fluid, this equation becomes :

$$\rho \frac{D\vec{U}}{Dt} = \rho\vec{g} - \nabla p + \mu\nabla^2\vec{U} \tag{3.2}$$

The gravity term is negligible in most cases. Thus the two–dimensional form of the Navier–Stokes equations for a constant property fluid are;

$$\frac{\partial u}{\partial t} + u\frac{\partial u}{\partial x} + v\frac{\partial u}{\partial y} = -\frac{1}{\rho}\frac{\partial p}{\partial x} + \nu\left[\frac{\partial^2 u}{\partial x^2} + \frac{\partial^2 u}{\partial y^2}\right] \tag{3.3}$$

$$\frac{\partial v}{\partial t} + u\frac{\partial v}{\partial x} + v\frac{\partial v}{\partial y} = -\frac{1}{\rho}\frac{\partial p}{\partial y} + \nu\left[\frac{\partial^2 v}{\partial x^2} + \frac{\partial^2 v}{\partial y^2}\right] \tag{3.4}$$

Taking the curl of these two equations and thus eliminating the pressure from them gives the "Vorticity Transport Equation" in two-dimension, that is

$$\frac{D\omega}{Dt} = \nu\nabla^2\omega \tag{3.5}$$

or

$$\frac{\partial\omega}{\partial t} + (\vec{U}.\nabla)\omega = \nu\nabla^2\omega \tag{3.6}$$

where "ω" is defined here as "fluid vorticity".

$$\omega = \frac{\partial v}{\partial x} - \frac{\partial u}{\partial y} \tag{3.7}$$

Consequently the incompressibility assumption $div\vec{U} = 0$, i.e.;

$$\frac{\partial u}{\partial x} + \frac{\partial v}{\partial y} = 0 \tag{3.8}$$

and definition of the stream function "ψ" as;

$$\frac{\partial\psi}{\partial y} = u \qquad\qquad \frac{\partial\psi}{\partial x} = -v \tag{3.9}$$

gives the Poisson's equation ;

$$\nabla^2\psi = -\omega \tag{3.10}$$

3.2 Splitting the Equations

The method proposed by Chorin [37] in connection with his work on "Slightly Viscous Flow Over a Circular Cylinder" is known as the "Operator Splitting","Time Splitting" or "Viscous Splitting" algorithm. In this method, at each time step one may solve the convection and diffusion of vorticity sequentially, rather than simultaneously, . For a two–dimensional flow, the Vorticity

Transport equation in the non–dimensionalized form, is

$$\frac{D\omega}{Dt} = \frac{1}{Re}\nabla^2\omega \tag{3.11}$$

where the Re is based on the cylinder diameter. But the method suggests to separate this equation into two parts as viscous diffusion

$$\frac{\partial\omega}{\partial t} = \frac{1}{Re}\nabla^2\omega \tag{3.12}$$

and convection

$$\frac{\partial\omega}{\partial t} = -(\vec{U}.\nabla)\omega \tag{3.13}$$

Denoting the solution operations of equation (3.12) and (3.13) as D(t) and C(t) respectively, one can mathematically write the description of viscous splitting algorithm which is applied at each of m time steps of duration Δt as

$$\omega(m\Delta t) = \{D(\Delta t)C(\Delta t)\}^m\omega(0) \tag{3.14}$$

Here, $\omega(m\Delta t)$ is the vorticity distribution after "m" step and $\omega(0)$ is the initial distribution [41] . The accuracy of the method is proved as converging to the Navier–Stokes solutions, under some restrictions by Beale and Majda [As referred to in 41]. Convergence of solution depends on the accuracies of convection and diffusion individually.[41]

3.3 Diffusion of Vorticity and Boundary Conditions on Circulation

In this study , the diffusion part of the vorticity transport equation is solved on the mesh. In two dimensions, non–dimensionalized form of the diffusion equation is;

$$\frac{\partial\omega}{\partial t} = \frac{1}{Re}\left[\frac{\partial^2\omega}{\partial x^2} + \frac{\partial^2\omega}{\partial y^2}\right] \tag{3.15}$$

where the Reynolds number is based on the cylinder diameter D and the free–stream velocity U_∞ i.e. $Re = U_\infty D/\nu$ Under transformation, this equation takes the form that includes the transformation modulus (Jacobian) between the computation and physical planes. Thus, using the mesh circulation values instead of vorticity which is assumed to spread uniformly in A, the diffusion equation can be written as follows;

$$\frac{\partial(\Gamma/A)}{\partial t} = \frac{1}{Re}\left[\frac{\partial^2(\Gamma/A)}{\partial x^2} + \frac{\partial^2(\Gamma/A)}{\partial y^2}\right]\left|\frac{d\xi}{dz}\right|^2 \tag{3.16}$$

The finite difference technique is applied to this equation with proper discretization allowing explicit calculations in –x direction and implicit in –y direction. The finite difference forms of this equation was given in Appendix A.

The diffusion equation is solved subject to the no–slip boundary condition at the surface. The first order approximation for the surface vorticity, in its circulation form [45] is employed.

$$\Gamma_w = -\frac{2(\psi_{w+1} - \psi_w)}{h}\Delta x \tag{3.17}$$

where "w" stands for the value at the wall, "$w+1$" for the neighbouring grid to the wall, "h" is the distance of the neighbouring grid to the wall and Δx is the constant mesh spacing in –x direction. Since the flow is impulsively started, the wall circulation values at the start of the motion are determined by the stream function values of the basic flow. As indicated by Roache higher degree of circulation boundary condition requires more computational time and for some cases improper results.

For the solution of the Poisson Equation for the stream function periodicity is imposed at the right and left boundaries of the computation plane ,and at the upper boundary the stream function values induced by the discrete vortices and their images in the body are taken as the boundary condition.At the lower boundary describing the wall,the stream function value is taken as zero. After calculating the diffused vorticity across the mesh and therefore determining the new vorticity field,the Poisson Equation is solved again and the stream function values at grid points are used to calculate the convection velocities of vortices.Consequently,the vortices are convected to their new positions at the end of each time step.

3.4 Convection of Vorticity

The method described above produces high number of discrete vortices in the flow field. The Vortex–in–Cell method employed in this study provides an effective way to calculate the convection velocities for these vortices.

In its simplest form ,the VIC technique requires allotment of circulation of each vortex occupying a cell to the four surrounding mesh points according to the bilinear area weighting scheme; in other words, the total circulation of a mesh point is defined by summing the contribution from all of the vortices resident in the four surrounding cells. If the circulation of a vortex is Γ, then the contribution of this vortex assigned to the four surrounding points on a cartesian mesh (Fig [3.1.(a)])is calculated by ;

$$\Gamma(i) = \frac{\Gamma . A_i}{\sum_{k=1}^{4} A_k} \tag{3.18}$$

This assignment gives the mesh circulations (i.e. the right hand side) used in the solution of Poisson's equation. With the stream function values determined from the solution of Poisson's equation (see section 3.5) the mesh velocities are calculated also taking into consideration the transformation moduli.

$$u = \frac{\partial \psi}{\partial y}\left|\frac{d\xi}{dz}\right|^2 \tag{3.19}$$

$$v = -\frac{\partial \psi}{\partial x}\left|\frac{d\xi}{dz}\right|^2 \tag{3.20}$$

Known the mesh velocities, an area weighting scheme, in reversed direction (Fig. [3.1.(b)]) then gives the convection velocities of the discrete vortices as follows;

$$u_p = \sum_{k=1}^{4} \frac{u(k)A_k}{A} \tag{3.21}$$

$$v_p = \sum_{k=1}^{4} \frac{v(k)A_k}{A} \tag{3.22}$$

where A is the total cell area. Consequently the vortices are advanced to their new locations , by a first order approximation:

$$x_p(t+\Delta t) = x_p(t) + u_p(t)\Delta t \tag{3.23}$$

$$y_p(t+\Delta t) = y_p(t) + v_p(t)\Delta t \tag{3.24}$$

where x_p and y_p are the orthogonal coordinates of vortex P, u_p and v_p are the velocities in –x and –y directions obtained at the previous calculation step.

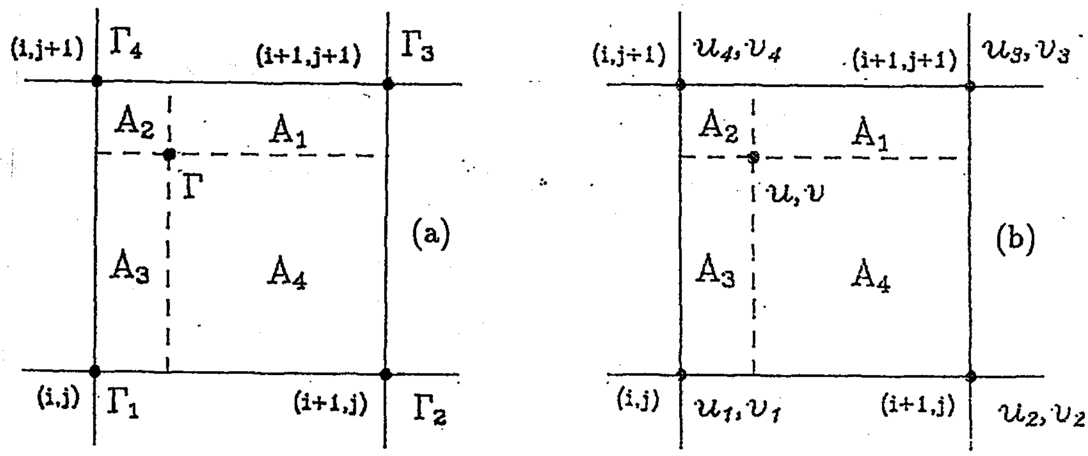

$$\Gamma_i = \Gamma . A_i / \sum_{k=1}^{4} A_k \qquad\qquad (u,v) = (u,v)_i . A_i / \sum_{k=1}^{4} A_k$$

Figure 3.1 Interpolation procedures for circulation and velocity

3.5 Solution of Poisson's Equation

Stream function values required to determine the convection velocities of the discrete vortices are obtained using Poisson's equation in its circulation form :

$$\nabla^2 \psi = -\frac{\Gamma}{A} \tag{3.25}$$

Many of the algorithms developed for the simple Poisson's equation fall into two apparently distinct categories: those based on Fourier decomposition in one dimension, using Fast Fourier Transform (FFT) techniques, and those based on block cyclic reduction. In the present study, the former is used. This brings a restriction on the type of solution domain, although some other direct methods do not: If the solution domain is a rectangular NxM grid, N, being the number of mesh points in x direction in which the Fourier transformation is taken, is restricted to be powers of 2, i.e. $N = 2^k (k = 1, 2, ...)$.

Taking the Fourier transform along –x direction reduces Poisson's equation into a tridiagonal system of equations. As described before, the boundary conditions at the top and bottom in transformation plane are given as Dirichlet type. For the surface, the stream function value is zero. On the other hand, the FFT technique used in this study asumes periodicity of stream function at the left and right boundaries. Since the Poisson's equation is a linear equation the superposition principle is applied and the stream function corresponding to a non–zero circulation distribution is added onto the stream function of the basic flow. (see section 3.7)

A detailed comparative study can be found in the review article of Temperton [46]. The discretized form of Poisson's equation is given in Appendix B.

3.6 Amalgamation of Vortices

For a number of reasons, in numerical studies with discrete vortices, amalgamation or merging of two or more vortices into a single one is a generally–resorted technique: Amalgamation

- can eliminate the unrealistically large velocities induced by the point vortices
- shorten the computing time by reducing the number of vortices, and
- can simulate some naturally occuring merging

By smearing the vortex onto a mesh it occupies, the VIC technique automatically eliminates the large velocities induced by the discrete vortices. However, due to production of large number vortices, the VIC technique without an amalgamation prodecure becomes computationally impractical.

Since the amalgamation is an approximation, there is no correct or guaranteed way to perform it. It should be used with care and, if possible, verified that it does not introduce unacceptably large errors. But unfortunately, it is difficult to assess the more elusive effects of merging on the numerical predictions since the problem is highly non–linear and its results depend on many different parameters which can easily be intermingled.

There are two merging schemes examined in this study . One of them is to associate the point vortex existing in a cell with the diffused vorticity at the four surrounding mesh points diffused vorticity without taking account their being like or unlike signed. Other one goes to a discrimination between like and unlike signed vortices. The oppositely signed vortices are combined when the distance between them is less than a prescribed value to mimic the cancellation of oppositely signed vorticity which is the major mechanism of enhanced energy dissipation in turbulent flow. This length is defined to be shorter than the one for the amalgamation of like signed vortices . When merging the like signed vortices the total circulation and linear momentum are conserved. But the second moment of vorticity distribution decreases and velocity fields before and after merging are not identical. This generally causes discontinities in the calculated force if either the generalized Blausius theorem or the time rate of change of first moment of circulation is used. Discrimination between like and unlike signed vortices gives large number of vortices thus increases the computing time although it is more accurate to simulate the viscous effects.

3.7 Solution Domain and Conformal Transformation

As a necessity of using hybrid scheme for flow computations, a proper grid should be produced around the body in order to simulate accurately the diffusion and convection processes. For a successful simulation, the grid should be fine enough to cover at least three or more meshes in the boundary layer [45]. To extend this fine grid structure into a region far from the body an impractically large number of grid points are required. However, since the large scale structures are the dominant feature of the flow far downstream, a coarser mesh is sufficient there. For the y locations of grid points the following expression is used:

$$y = \frac{A + \sqrt{A^2 + 4BC(J-1)}}{2B} \tag{3.26}$$

where A=J-1-D. By assigning different values to the parameters B,C,D , various grid structures can be produced in the transformation plane which provides different definitions in the boundary layer and different locations for the outer boundary of the computational domain.

The transformation between the computation (rectangular) and the physical domains is achieved in two stages:

- First, the transformation from semi-infinite plane to plain cylinder and
- Secondly the transformation from plain cylinder to circular cylinder with splitter plate attached to its end.

These stages are described as follow:

Stage 1– Transformation from semi-infinite plane to plain cylinder

Calling semi-infinite plane as "ξ" plane, plain cylinder plane as "ζ" plane , the expression for this conformal transformation is;

$$\zeta = R\exp(-i\alpha\xi) \tag{3.27}$$

where ζ and ξ represent complex coordinates

$$\zeta = \zeta_R + i\zeta_I, \qquad \xi = \xi_R + i\xi_I \tag{3.28}$$

in semi–infinite plane and the plain cylinder plane respectively and R is the radius of cylinder and α is step size in angular direction. For this stage, the differential quotient of the mapping funtion is;

$$\frac{d\zeta}{d\xi} = -i\alpha R\exp(-i\alpha\xi) \tag{3.29}$$

Stage 2– Transformation from plain cylinder to cylinder with splitter plate

Conformal transformation between these two planes also used by Çete [47] is as follows:

$$z = F \pm \sqrt{F^2 - 1} \tag{3.30}$$

where

$$F = \frac{(1 + L_p)^2}{8L_p}\left(\zeta + \frac{1}{\zeta}\right) \tag{3.31}$$

where L_p is the length of the splitter plate measured from the center of the cylinder. z represents the complex coordinate in the physical plane (i.e. circular cylinder with a splitter plate attached to its end) , and the corresponding differential quotient of the mapping function is

$$\frac{dz}{d\zeta} = \frac{(1 + L_p)^2}{8L_p}\left(1 - \frac{1}{\zeta^2}\right) \pm \left[\frac{\sqrt{F^2 - 1} + F}{\sqrt{F^2 - 1}}\right] \tag{3.32}$$

From foregoing expressions, the global differential quotients of the composite mapping is the product of these two quotients. That is;

$$\frac{dz}{d\xi} = \frac{dz}{d\zeta}\frac{d\zeta}{d\xi} \tag{3.33}$$

The stream function of the basic flow around a circular cylinder placed in a uniform flow can be easily expressed in the intermediate plane of circular cylinder . However, in order to determine the corresponding basic flow in the physical plane this stream function expression should be multiplied by the limit value of the differential quotient of the transformation passing from physical plane to the intermediate one (i.e. plain cylinder plane). The limit, as ζ goes to infinity, is;

$$\lim_{\zeta \to \infty} \frac{dz}{d\zeta} = \frac{4L}{(1 + L_p)^2} \tag{3.34}$$

3.8 Force Calculation

Force due to the vortex shedding is determined by the total rate of change of first moment of circulation. Approach is applicable to viscous flows as well as inviscid flows [48]. Therefore the expression for the vortex force is

$$F_v = -i\rho \frac{d\beta}{dt} \tag{3.35}$$

where β is the first moment of vorticity field:

$$\alpha = \int_{R_L} \vec{r} \times \vec{\Omega} dR \tag{3.36}$$

and $\vec{r}$ is the position of the vortex; R_L includes all the region outside of the body. Consequently the discrete version of the force expression in terms of mesh circulation Γ_k can be written as follows;

$$F_v = -i\rho \frac{\partial}{\partial t} \sum_{k=1}^{N} \Gamma_k z_k \tag{3.37}$$

where z_k is the physical plane complex coordinates. Actually, the mesh points do not change with time but circulations do. Thus the equation takes the following form;

$$F_v = -i\rho \sum_{k=1}^{N} z_k \frac{\partial}{\partial t} \Gamma_k \tag{3.38}$$

Dimensionless force coefficient follows as;

$$C_{fv} = \frac{F_v}{\frac{1}{2}\rho U^2 d} \tag{3.39}$$

where U is the free stream velocity and d is the cylinder diameter. The real and imaginary parts of this expression are dimensionless drag (C_D) and lift (C_L) coefficients respectively.

The flow diagram of the time–splitting solution of the Navier–Stokes eqautions is given in Fig. [3.2]

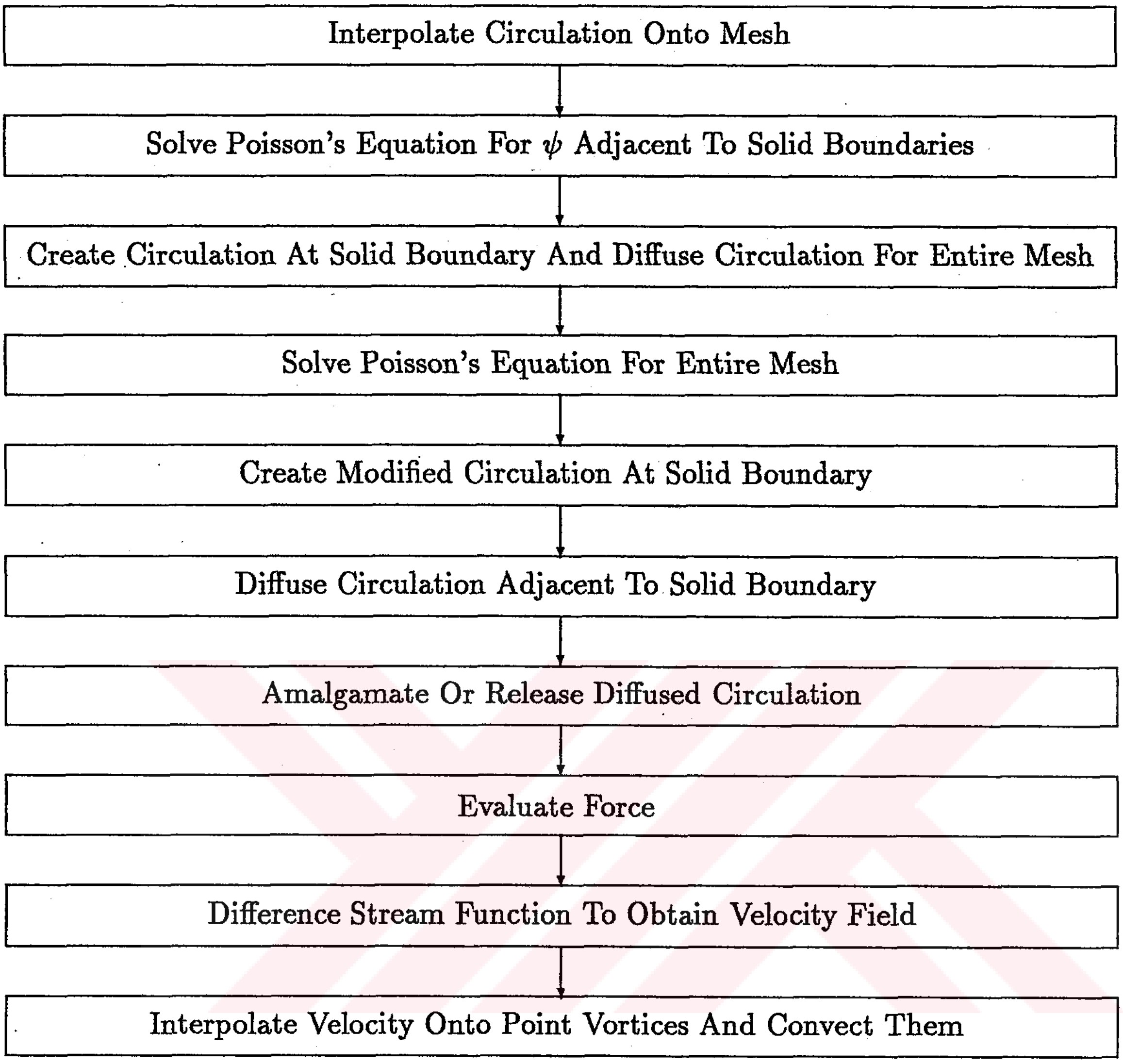

Fig. 3.2 Flow diagram of Convective–Diffusive Solution of Navier Stokes Equations

CHAPTER 4

RESULTS AND CONCLUSION

4.1 Choice of Run Parameters

In setting up the computational model of a real system, the determination of computational parameters such as the Reynolds number, the size of the integration time step mesh cells constitutes the first problem. Of course, the grid should be fine enough and the time step sufficiently small so that increased temporal or spatial resolution will not affect the results.

The grid dependent hybrid method employed in this study requires a proper grid to calculate the velocity field through the use of Poisson's equation, and to solve the diffusion part of the vorticity transport equation. In close neighbourhood of the body, the grid must be fine enough for representation of the boundary layer accurately. On the other hand, the grid should extend far enough in streamwise direction so that the rotational fluid cannot reach to the outer boundary of the solution domain during the calculations . All of the computations are carried out in a rectangular domain obtained conformally transforming the physical flow domain (i.e., the region outside of the circular cylinder with a splitter plate attached to its end) [Fig. 4.1]. The above mentioned constraints lead to a grid expanding in direction perpendicular to the lower boundary of the rectangular domain (in –y direction) corresponding to the body boundary. Whereas, in direction parallel to the lower boundary (in –x direction), a constant spacing is employed in order to obtain a numerical solution of Poisson's equation by making use of Fast Fourier Transformation Technique. The rate of expansion of the cell size in –y direction is choosen to be less than 1.2. The grid structure staisfying these restrictions is shown in Fig. [4.1.(b)], whereas Fig. 4.1.(a) shows the corresponding grid structure in the physical plane for which the splitter plate length L with respect to the cylinder diameter D is $L/D = 1$. In the computational plane, ratio of the successive mesh spacings is not greater than 1.15 and the number of mesh points is 128 in –x direction and 40 in –y direction. This grid structure, having 4 points within the boundary layer was considered sufficient for calculations at $Re = 500$.

After setting up the grid structure, the size of integration time step has been determined. In doing this, the diffusive stability criterion is considered. For the case of diffusion, the stability criterion is that the amount of vorticity diffused from a mesh point onto the surrounding four mesh points must in total be less than the original vorticity at that mesh point. Otherwise, it is possible to have a point that diffuses more than its own value of vorticity away from the point, which at the next time step would be diffused back onto the point, allowing a mechanism of unstable vorticity growth in the fluid itself [49]. For a regular square mesh this condition can be represented as

$$\frac{\delta t}{Re}\nabla_z^2\omega = \frac{\delta t}{Re}\nabla_\zeta^2\omega \left|\frac{d\zeta}{dz}\right|^2 < \frac{\omega}{4} \qquad (4.1)$$

Table 4.1 On this table, NX and MY are the number of grid points in –x and –y directions respectively and J_{min} is the minimum value of transformation modulus.

L/D	NX	MY	Δt	J^2_{min}	Δy_{wall}	Δx
0	128	40	0.005	.243	0.1	0.1
0.25				$2.4.10^{-3}$		
0.5				$1.5.10^{-3}$		
1				$1.5.10^{-3}$		
1.5				2.10^{-3}		
2				$2.4.10^{-3}$		
2.5				3.10^{-3}		

Taking the worst case computed here (non–dimensional splitter plate length L/D=0.5 and 1 giving $J^2_{min} = 1.5 \times 10^{-3}$, (Table 4.1) gives an upper bound of 0.00094 on the time step. However, this is prohibitively small time step for the PC with 486 co–processor used in this study. Therefore, time step for the calculations is taken to be 0.005. Effect of taking time step according to the stability criteria is still under investigation.

4.2 Circular Cylinder Without Splitter Plate

Vast amount of illuminating investigations into the case of flow around a circular cylinder ([15] and [50] to [57]) provides an excellent grounds for comparison of and testing the code used in this study. The code has been examined according to the run parameters such as the time step Δt, mesh spacings and number of grid points in –x direction in the computation plane.

4.2.1 Time Step Comparisons

For 64 grid points in –x direction five different time steps were considered. Fig. [4.2] and Fig. [4.3] show the variations with respect to time of the drag and lift coefficients as a function of integration time step. According to the above mentioned stability criteria the upper limit of time step for the plain cylinder is 0.15. Therefore, all of the time steps considered satisfy the criteria. However, for smaller time steps, drag coefficient shows a noisy variation. Additionally, the mean value of the drag coefficient increases, whereas there is not much variation in the fluctuation amlitude of the lift coefficient. The mean value of the drag coefficient is a little less than 1 and the lift coefficient fluctuates around zero mean value with an amplitude of approximately 1.5. Passing from $\Delta t = 0.01$ to 0.005 not much variation is observed either in the mean value of the drag coefficient or the periodicity and amplitude of the lift coefficient fluctuation. Therefore 0.005 is considered as a sufficiently small value for the time step.

4.2.2 Mesh Spacing Comparisons

For this phase of the study a fixed time step $\Delta t = 0.005$ is used. Here the critical parameter is the minimum mesh spacings in –y direction (Δy_{wall}) in the computation plane. Variations in the drag and lift coefficients with respect to time are compared for five different values of Δy_{wall} parameter. For all cases, the number of grid points in –x direction is 128. The grid generation procedure (please refer to section 3.7) in this study is such that for small values of Δy_{wall}, rate of expansion of the grid spacing in –y direction is larger. Therefore, smaller mesh spacing in the immediate neighbourhood of the body boundary implies large grid spacings in the region far downstream. Consequently, the accuracy of transport of vorticity in the region downstream of the cylinder greatly reduces. This is especially evident in the lift coefficient variation for small Δy_{wall} values (e.g. $\Delta y_{wall} = 0.04$) : There is a considerable deviation in the mean value of the lift coefficient from zero value. Additionally, the mean value of drag coefficient is unrealisticly low for the values of Δy_{wall} smaller than 0.1. Consequently, the value of smaller mesh spacings employed in the rest of the study is decided to be 0.1.

4.3 Circular Cylinder With The Splitter Plate

For this case the grid structure examined for the plain cylinder case is employed. As mentioned above, due to the limitation put by even the most powerfull computer available in our faculty, the time step is taken to be 0.005 which is larger than that the diffusive stability criteria indicates. For 128 grid, this value of time step requires about 36 hours for one case to be completed. It should also be indicated that the transformation from a perfect circular cylinder with a zero–thickness splitter plate attached to its end present singularities. Fitting a small envelope around this geometry, the singularities are left aside and therefore the flow considered in this study actually takes place around this envelope. (See e.g. Fig. [4.1.(a)]).

4.4 Discussion of Results

Results of the time splitting algorithm at $Re = 500$ are obtained for 6 different splitter plate lengths as well as for the plain cylinder case. The splitter plate lengths are $L/D = 0.25, 0.50, 1.00, 1.50, 2.00 and 2.50$. The experimental studies by Apelt et.al.[27] and Gerrard [7] forms a basis of comparison. Up to date, apart from that of Kawai [58] no numerical study into the effect of splitter plate on a circular cylinder wake has been encountered in the literature. Kawai, by representing the splitter plate with a series of sources, makes a Lagrangian Discrete Vortex Approach to the flow configuration considered in this study. He applied a heuristic model for a circulation reduction and found a Strouhal number variation with respect to the splitter plate length that is in qualitative agreement with experiments. Herein, it is hoped that the application of the viscous discrete vortex method will increase our understanding of the underlying physics of the flow.

Figures [4.6] and [4.7] show the streamline patterns and discrete vortex distributions for varying splitter plate length L/D. In Fig [4.6] streamlines are drawn with an increment of $\Delta\psi = 0.1$. Fig. [4.8] shows the color–coded streamlines corresponding to the cases given in Fig. [4.6], while Fig. [4.9] provides information about the vorticity distributions as a function of the splitter plate length . For comparison, the pictures are taken when the fluctuating lift force passes through a minimum in each case. The observed variations of the flow structures with the splitter plate lengths is in accord with those revealed by the experimental study by Apelt et.al.[27]: The formation of the vortex for the cylinder without the splitter plate takes place in region very close to the base of the cylinder . With increasing plate length, the vortex formation is delayed until the end of the plate and the travelling of the vortex accross the centerline is gradually eliminated. As the plate length increases from $L/D = 1.5$ to 2 the formation length of the vortex somewhat reduces. However, passing from $L/D = 2$ to 2.5 an increase in the formation length is observed. As evident from the longitudinal spacings between the large scale vortices in the vortex street wake (Fig. [4.7]), Strouhal number first decreases and then increases with increasing splitter plate length. Variation of Strouhäl number as a function of L/D can be calculated by means of the Fourier analysis of the fluctuating lift force vs. time (Fig. [4.14]). Fig. [4.10] shows the values obtained by such an analysis. In conformity with experiments ([27],[7]) St number passes through a minimum at around $L/D = 1.0$ and for longer plate lengths recovers to values close to that for the plain cylinder case. However, the predicted St numbers for the intermediate plate lengths are much lower than those obtained experimentally at $Re = 10^4$ [27]

There is a better agreement in the drag coefficient variation with respect to the splitter plate length (Fig. [4.11]). The mean values of drag coefficients values are obtained by time averaging of the drag coefficient variations with respect to time (Fig. [4.13]). In doing this the part of the variation after non–dimensional time $T = 50$ is considered. As seen in Fig. [4.11] the mean value of drag coefficient sharply reduces close to a third of the plain cylinder value. This sharp reduction is followed by a gradual one with increasing plate length and in contrast to the experiment by Apelt et.al. no recovery of the mean value of the drag coefficient is predicted for the plate length $L/D = 2.0$

As to the fluctuating lift force (Fig. [4.14]), the fluctuation amplitude steadily increases with increasing plate length. The variation of the amplitude of fluctuation of the lift coefficient with respect to splitter plate length is given in Fig. [4.12].

An interesting feature that has not been reported in the literature before is the appearance of secondary vortex developing from the tip of the splitter plate. As evident in figures [4.15] to [4.18] this evolution is seen once a period of vortex shedding and depending on the splitter plate length has different phase relations with the neighbouring large scale vortex. As mentioned in the above, increase in the length of the formation region with increasing plate length does not take place indefinitely; after a certain plate length the vortices completes the evolution before the end of the plate. Consequently depending on the splitter plate length large and small scale (tip vortex) vortices can be like– or unlike–signed. When the large scale vortex reaches to the end of the plate, interaction between these vortices is expected to lead to a large scale of varying strength depending on the plate length. For instance for $L/D = 0.25, 0.50, 1.0$ and 1.50 a positively signed large scale vortex co–exist with a tip vortex of opposite sign whereas for $L/D = 2.0$ vortices of like sign meet at the plate. This interaction can be a possible mechanism responsible for the above mentioned Strouhal number variation with the splitter plate length.

4.5 Conclusion

In this study, the aim has been to simulate and thus increase our understanding of the physics of the flow around a circular cylinder with a splitter plate length attached to its base. Results obtained show qualitative agreement with those found by experiments.

An interesting feature observed in this study is the appearance of a secondary vortex formation from the tip of the splitter plate and its interaction with the large scale vortex formed from the cylinder. This interaction varies depending on the splitter plate length and may be an important part of the mechanism responsible for the variation in the wake characteristics with plate length. This feature deserves further attention.

(a)

(b)

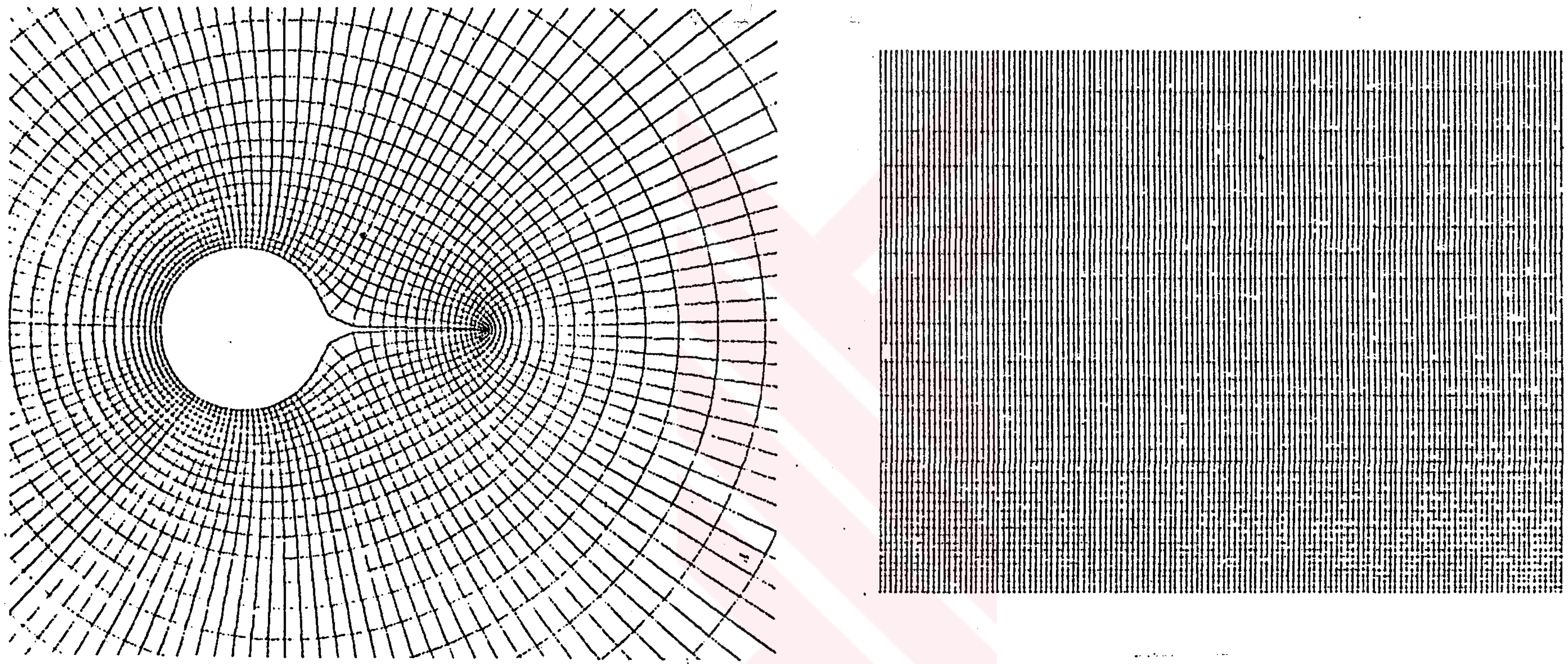

Fig.4.1 Grid structures in physical (a) and transformation (computation) plane (b)

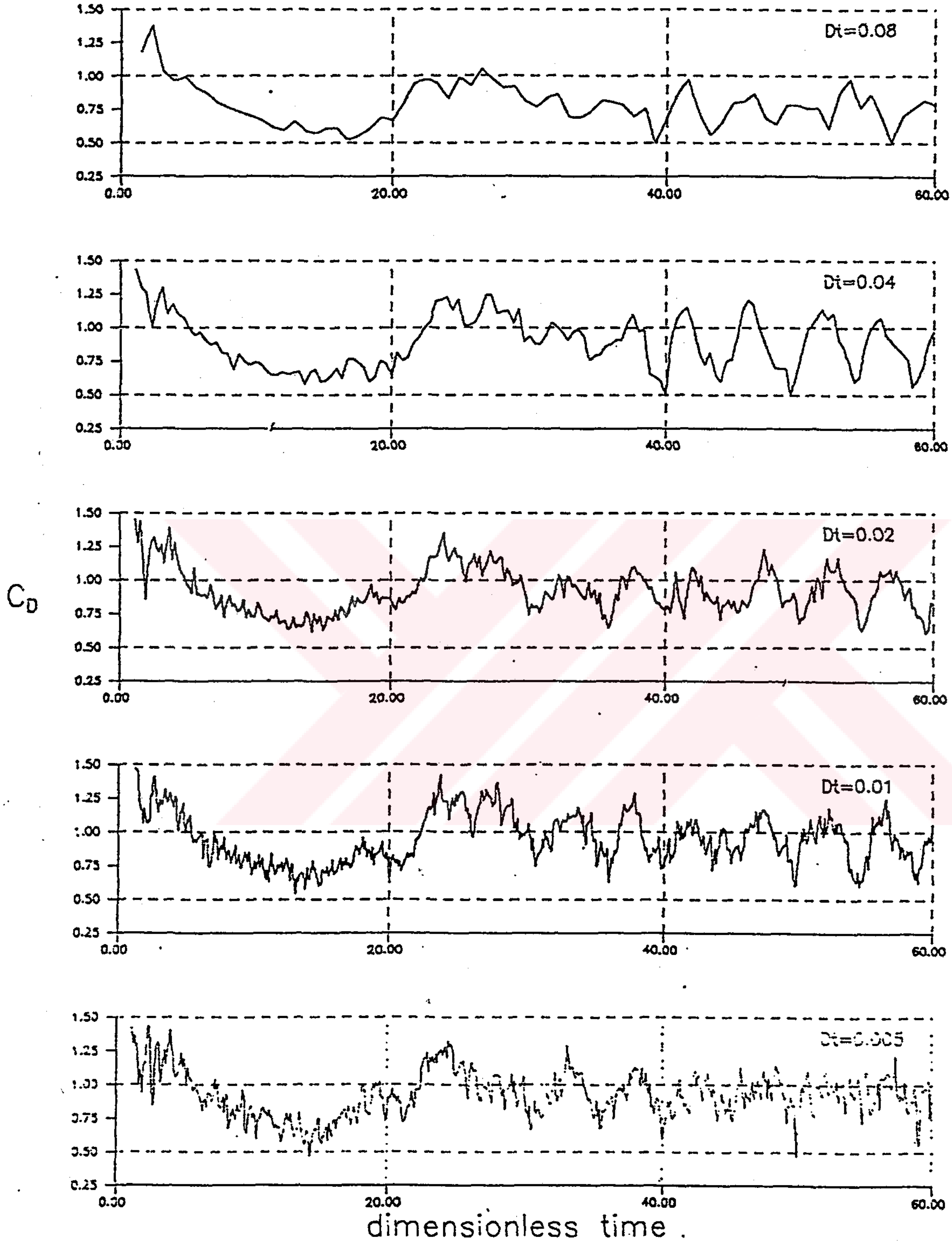

Fig. 4.2 Variation of drag coefficient C_D vs time with respect to different time steps (Δt).

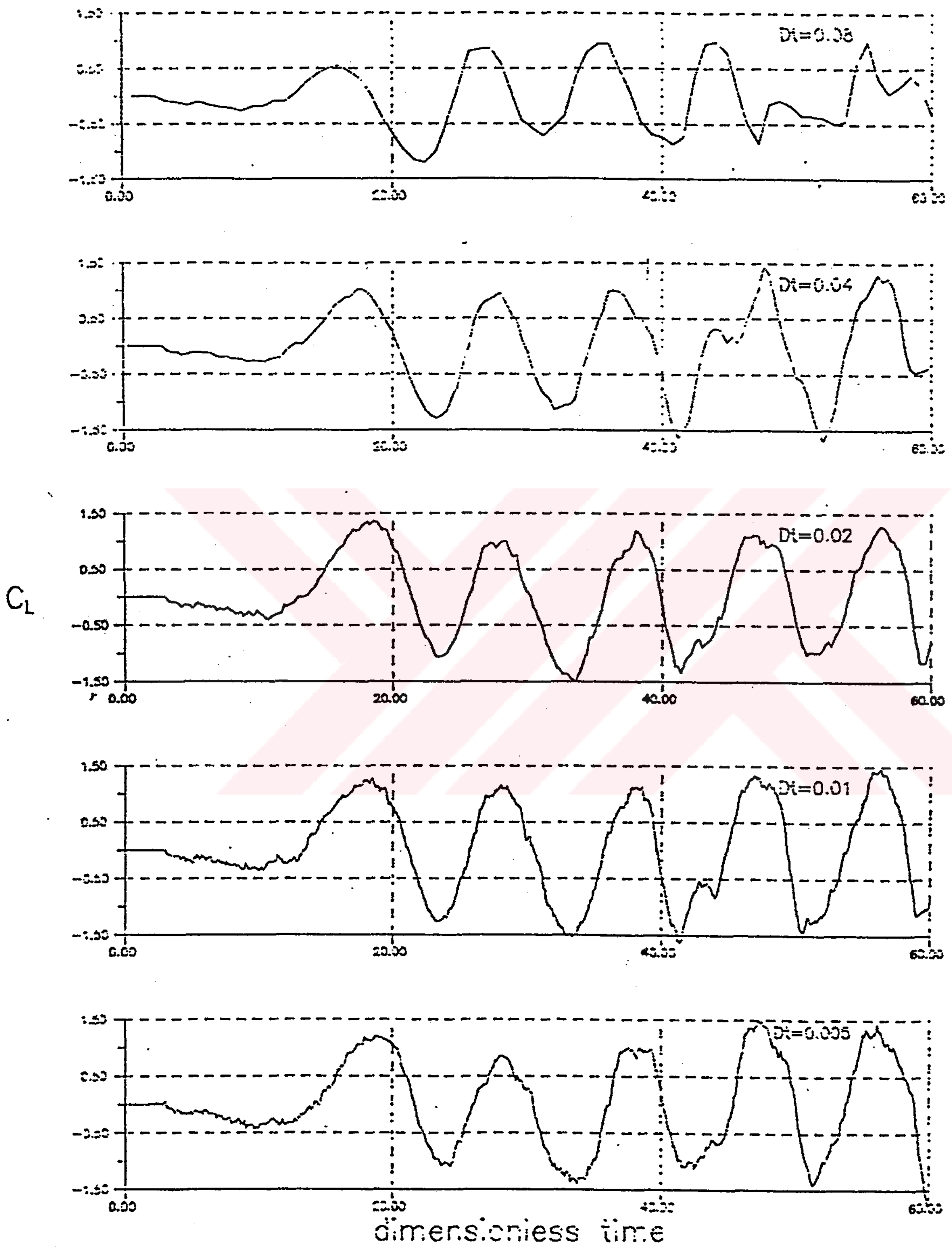

Fig. 4.3 Variation of lift coefficient C_L vs time with respect to different time steps.

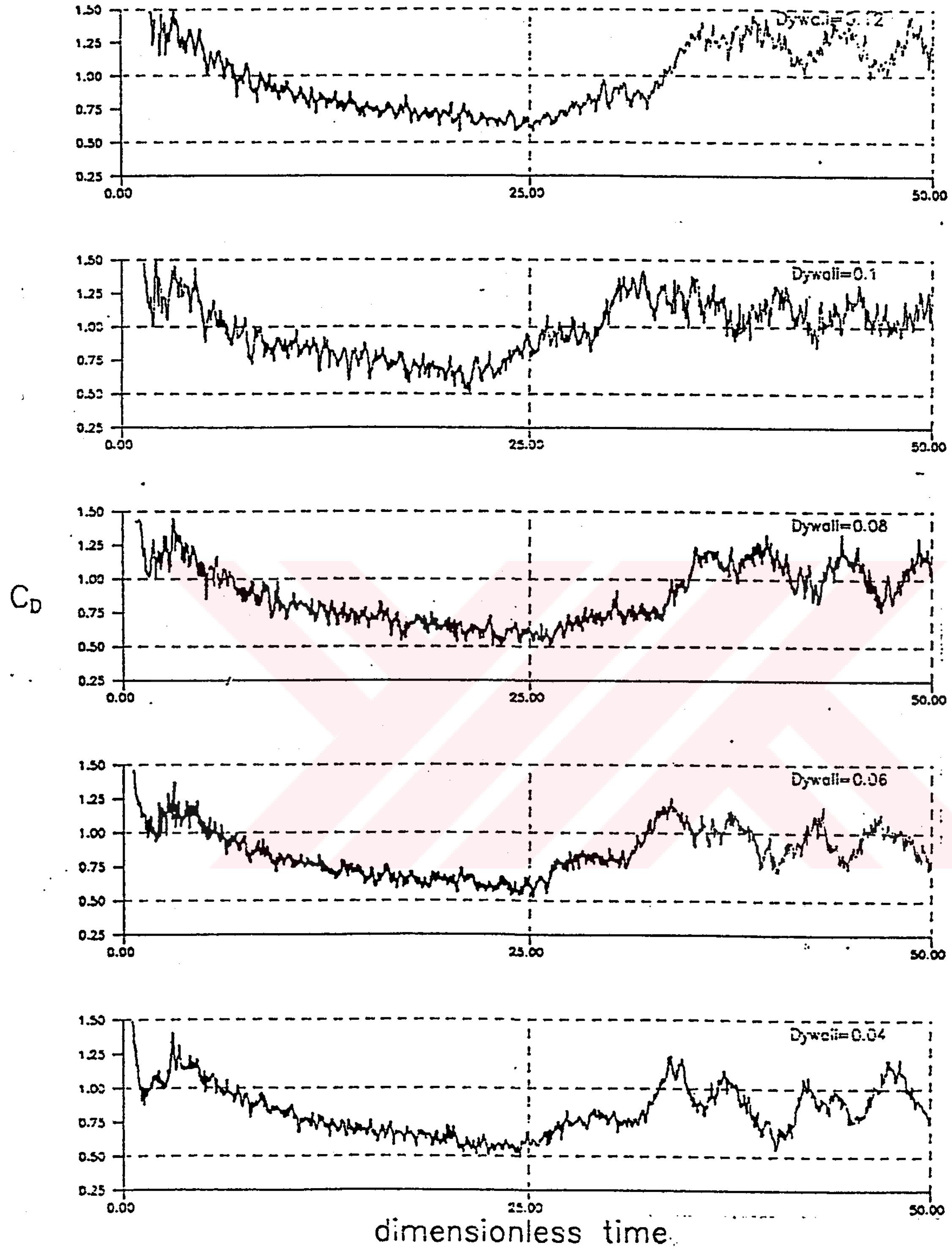

Fig. 4.4 Variation of drag coefficient C_D vs time with respect to values of minimum mesh spacing (Δy_{wall}) .

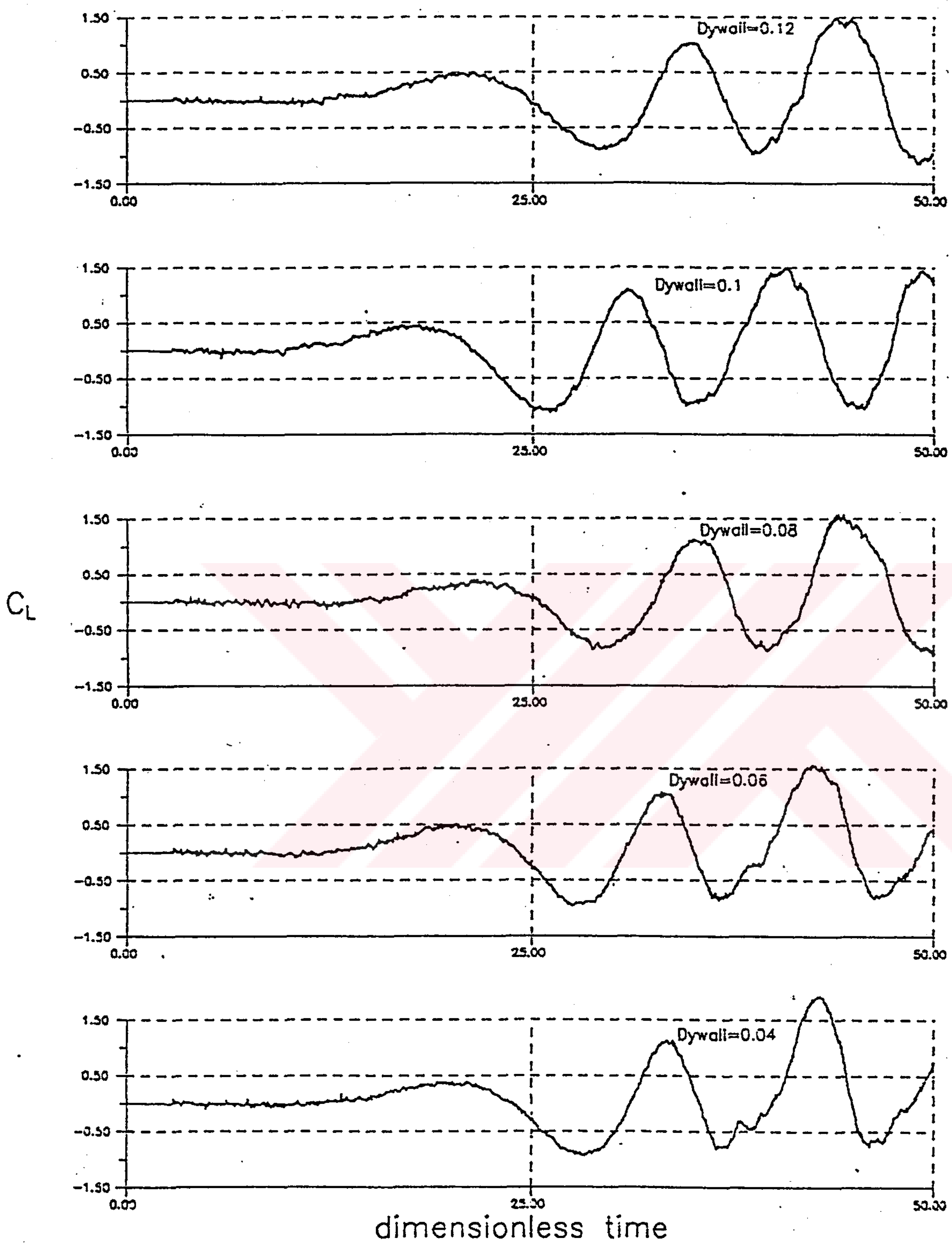

Fig. 4.5 Variation of lift coefficient C_L vs time with respect to values of minimum mesh spacing (Δy_{wall}).

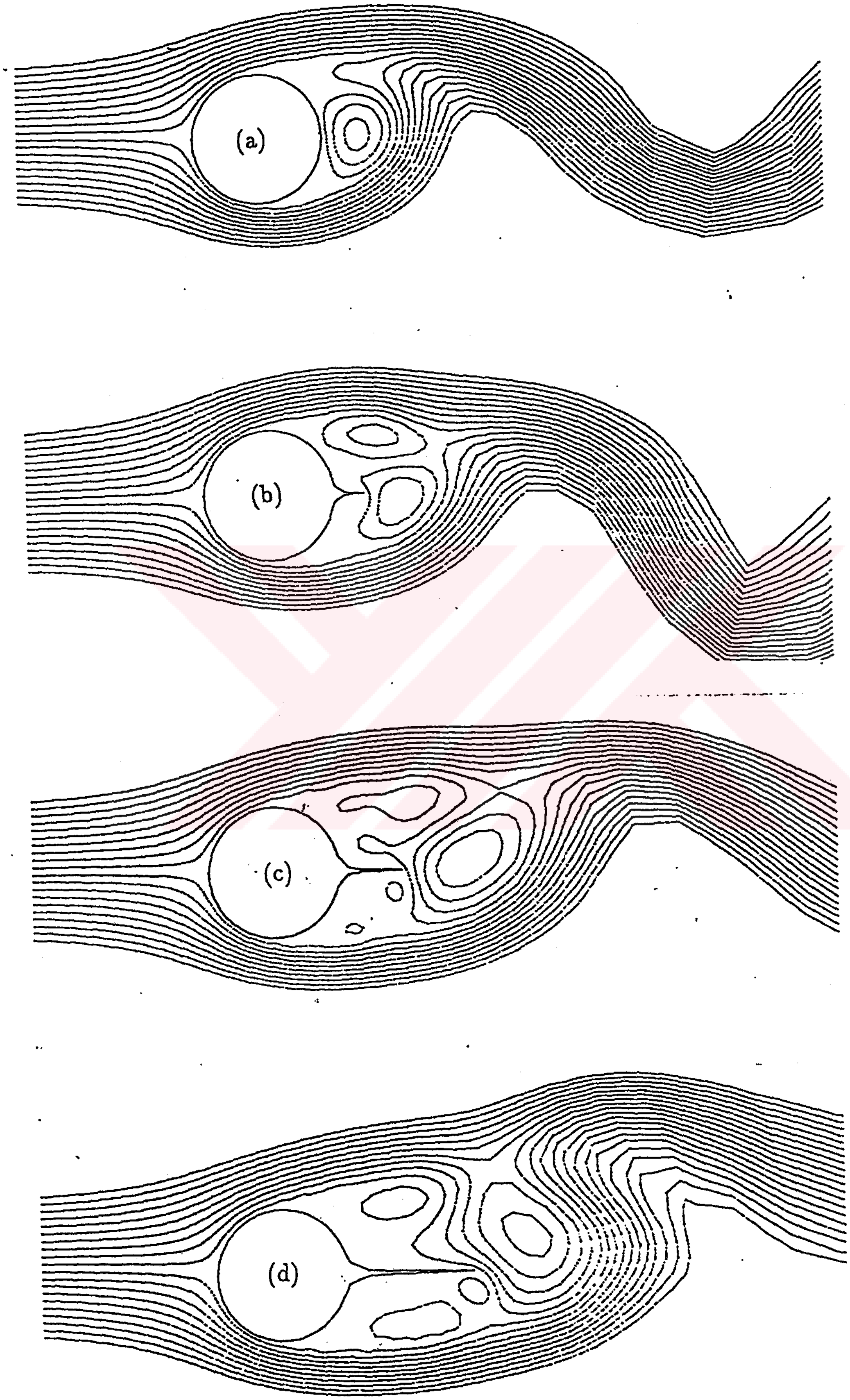

(For legend see next page)

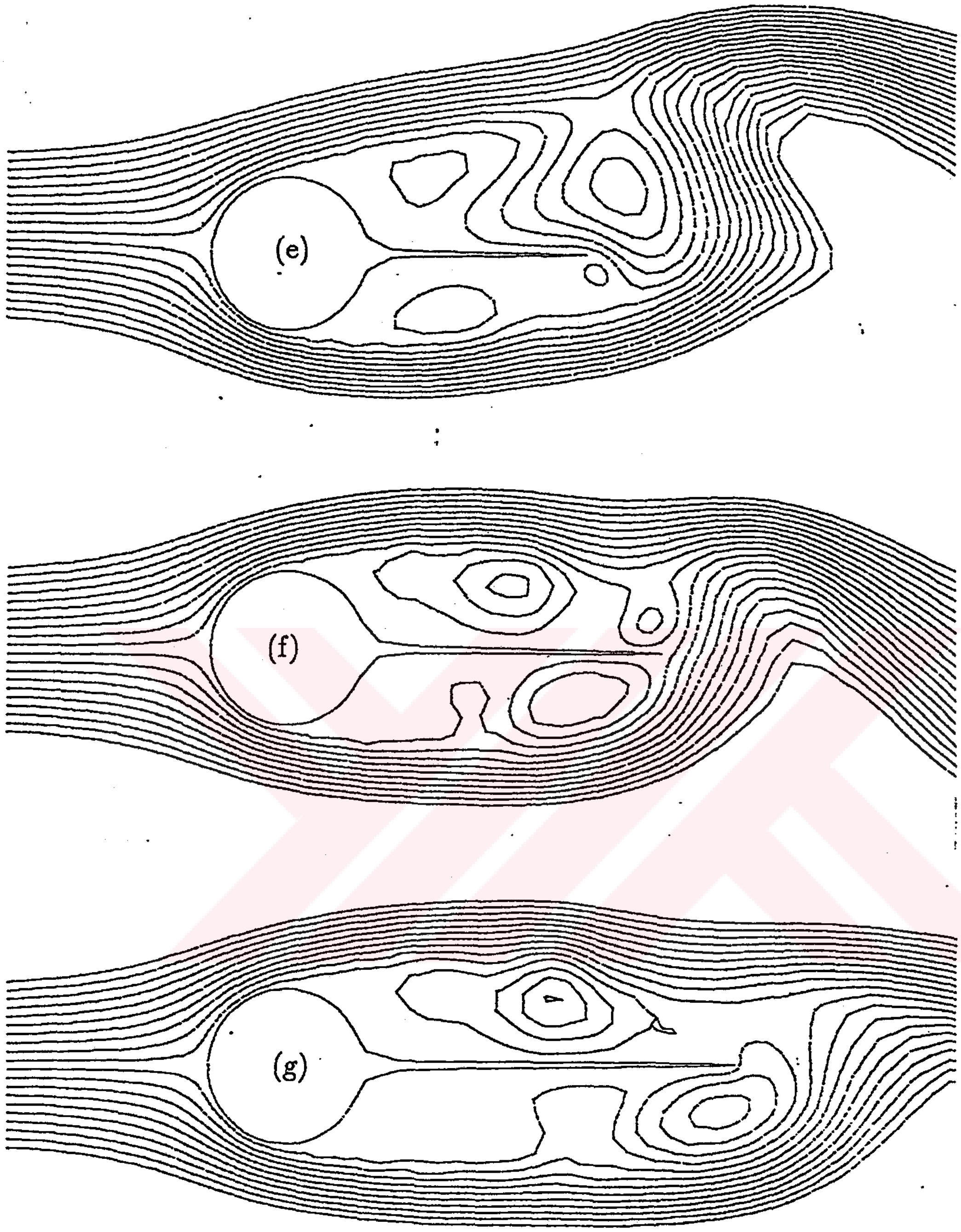

Fig. 4.6 Streamline patterns for L/D=0(a),0.25(b),0.5(c),1(d),1.5(e),2(f),2.5(g) when fluctuating lift force passes through a minimum.

(For legend see page 54)

(For legend see page 54)

(For legend see next page)

Fig. 4.7 Discrete vortex distributions for L/D=0(a),0.25(b),0.5(c),1(d),1.5(e),2(f),2.5(g) corresponding to the cases in Fig. 4.6.

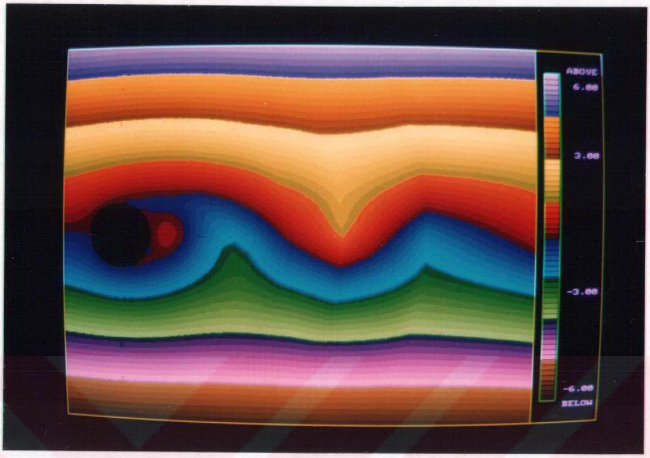

(a)

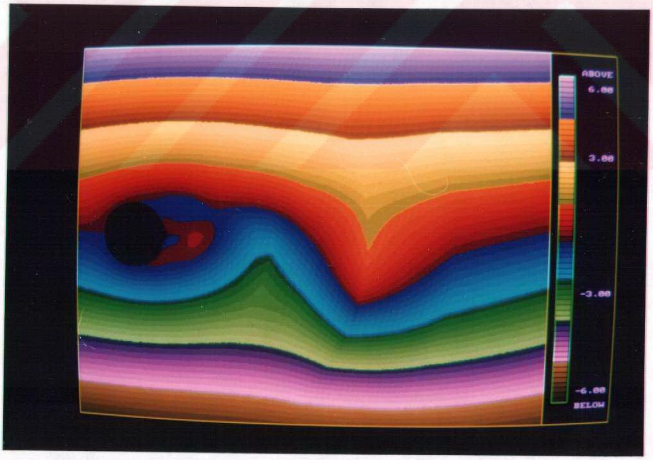

(b)

(For legend see page 58)

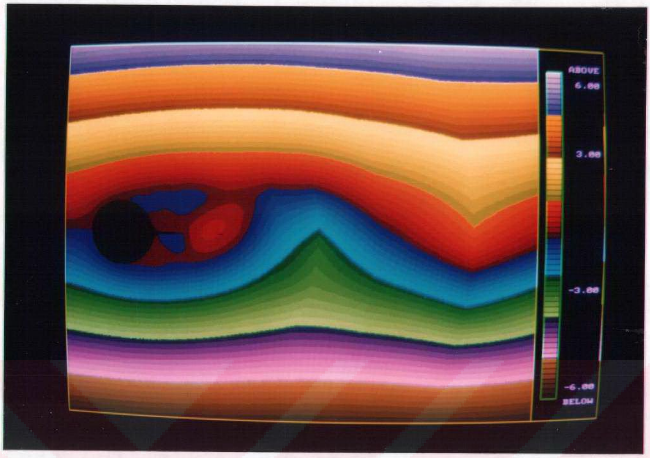

(c)

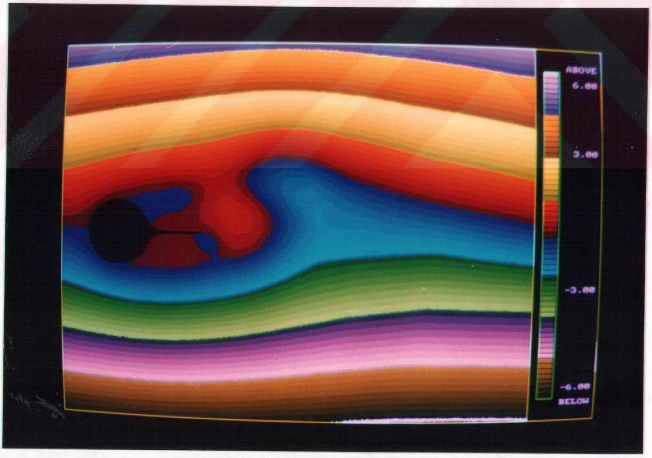

(d)

(For legend see page 58)

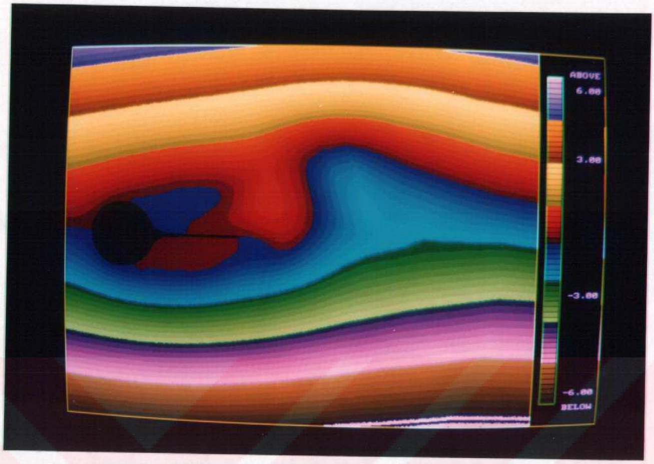

(e)

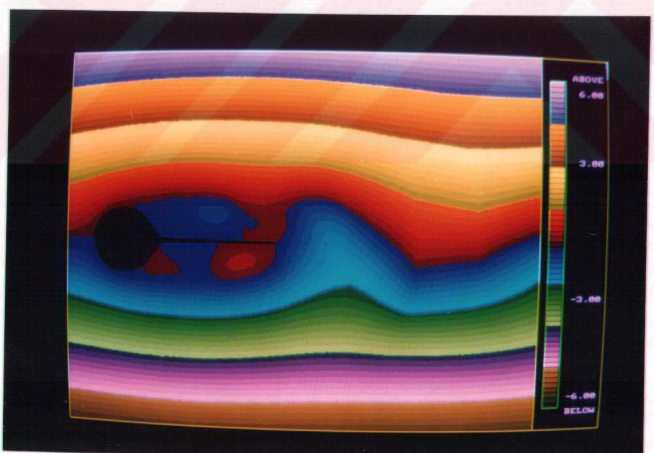

(f)

(For legend see next page)

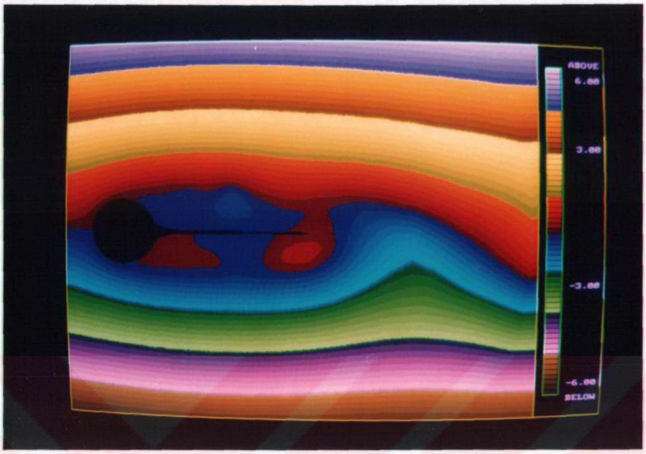

(g)

Figure 4.8 Color coded streamlines corresponding to the cases in Fig 4.6

(a)

(b)

(For legend see page 62)

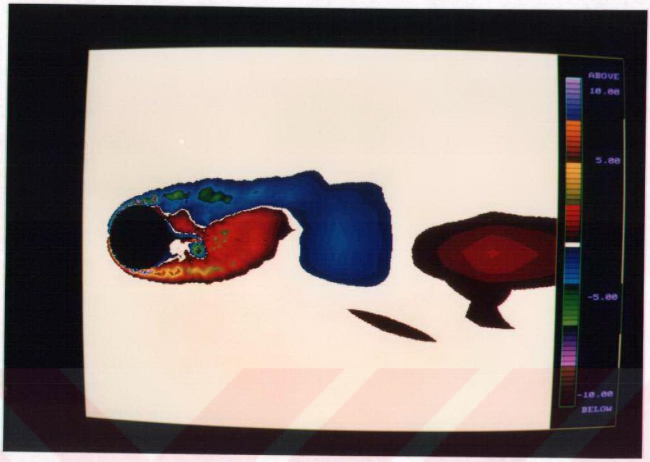

(c)

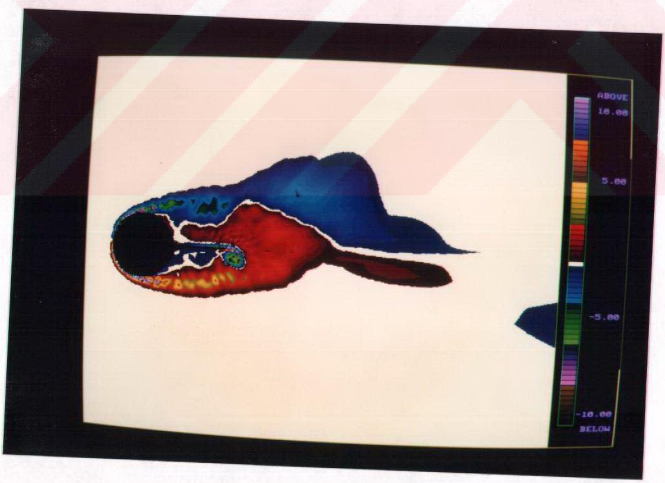

(d)

(For legend see page 62)

(e)

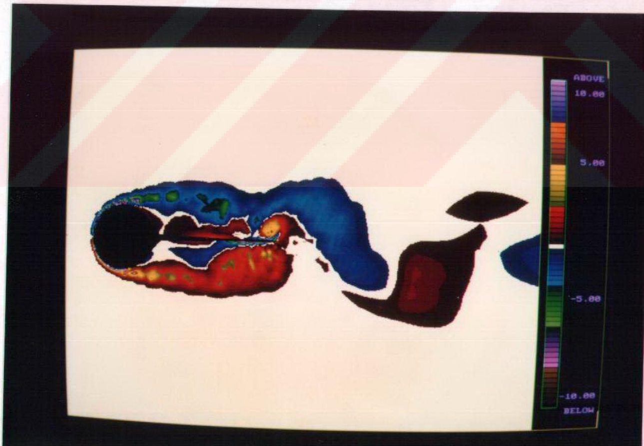

(f)

(For legend see next page)

(g)

Figure 4.9 Color coded vorticity distributions corresponding to the cases in Fig 4.6

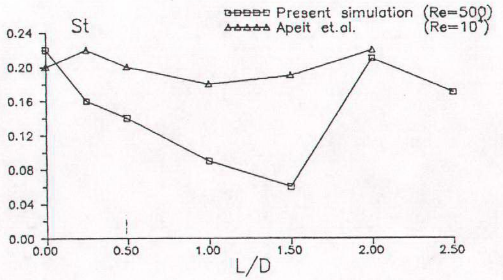

Fig. 4.10 Strouhal number variation vs L/D.

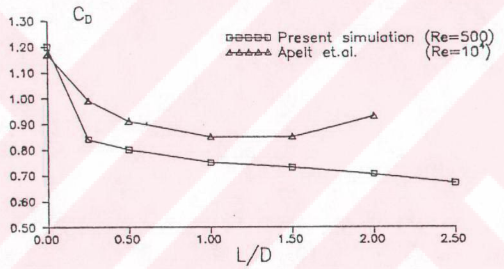

Fig. 4.11 Drag coefficient variation vs L/D.

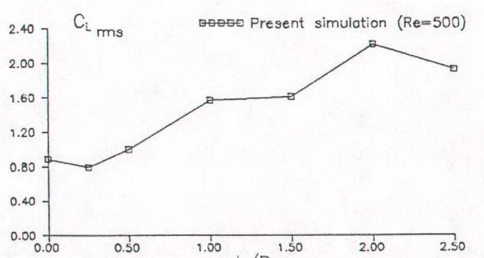

Fig. 4.12 Amplitude of lift coefficient fluctuation vs L/D.

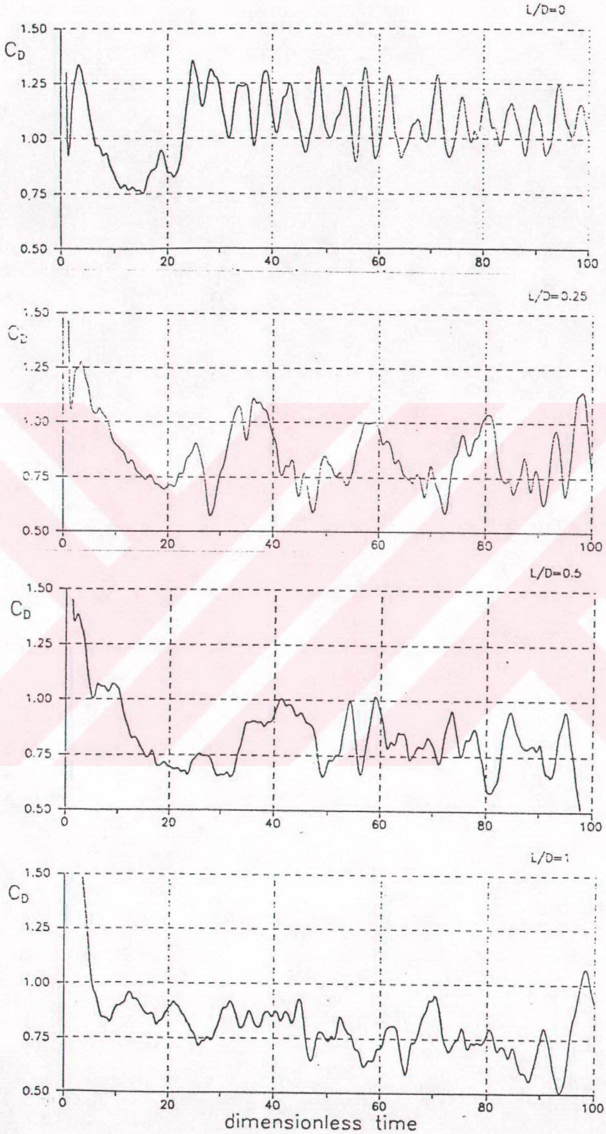

(a)

(b)

(c)

(d)

(For legend see next page)

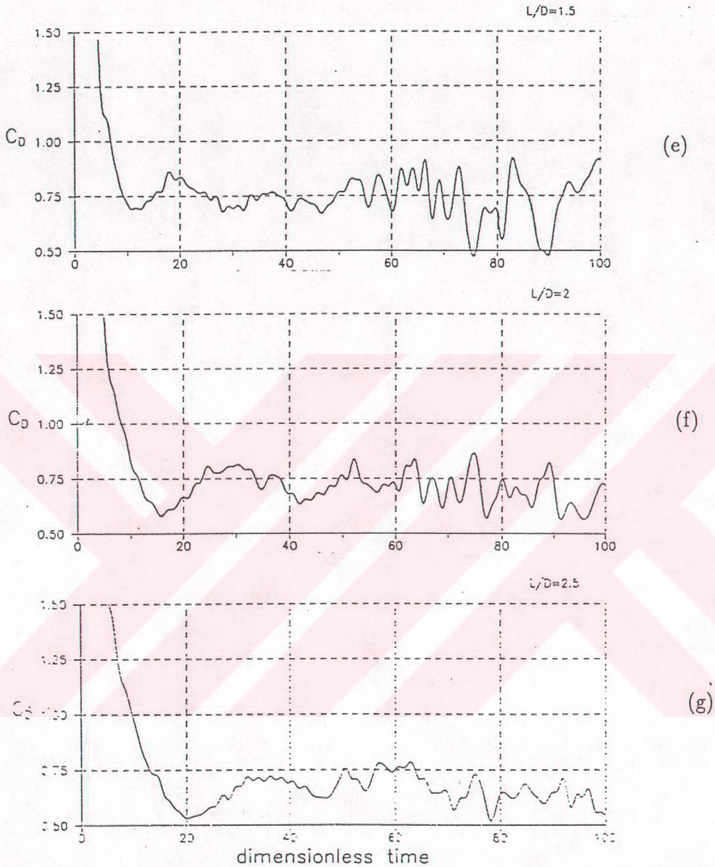

Fig. 4.13 Drag coefficient variation vs time with respect to splitter plate length ,

L/D=0(a);0.25(b);0.5(c);1(d);1.5(e);2(f);2.5(g)

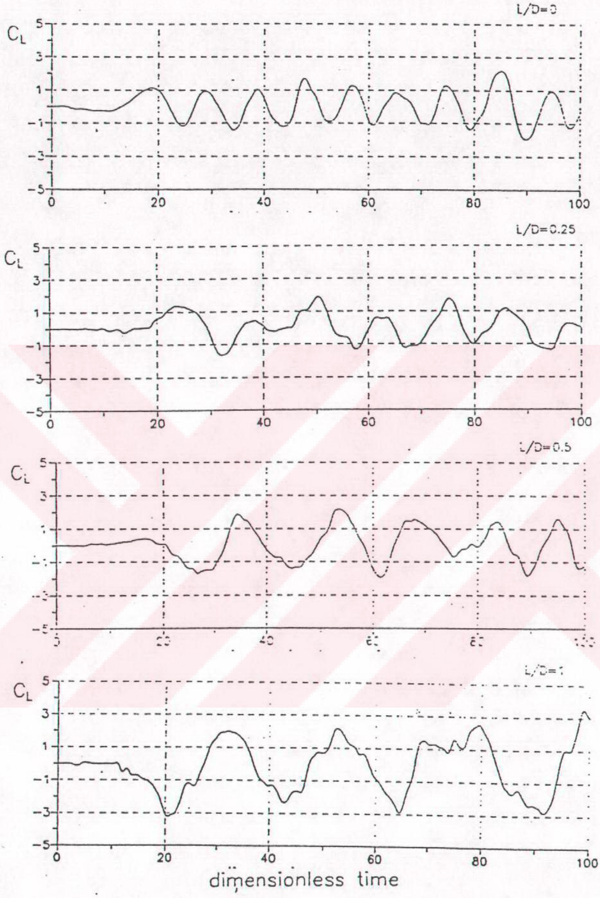

(a)

(b)

(c)

(d)

(For legend see next page)

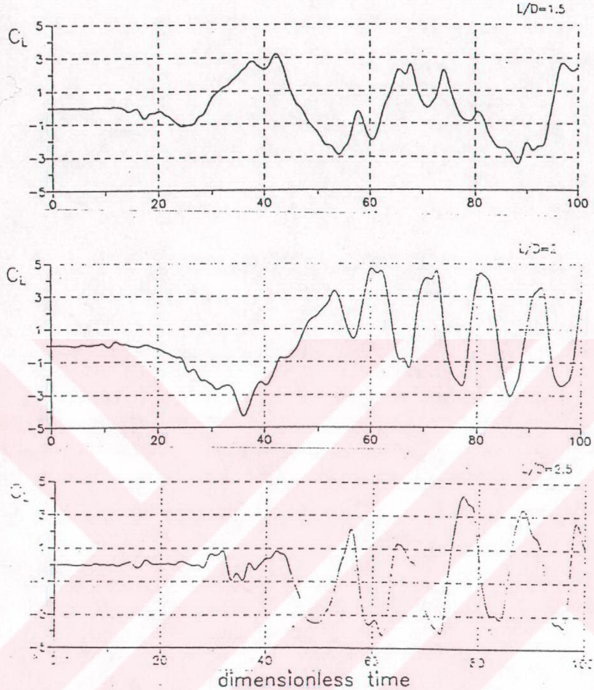

(e)

(f)

(g)

Fig. 4.14 Lift coefficient variation vs time with respect to splitter plate length, L/D=0(a);0.25(b);0.5(c);1(d);1.5(e);2(f);2.5(g)

Fig. 4.15 One period (from a minimum to next minimum in fluctuating lift force) for L/D=0.25.

(a)

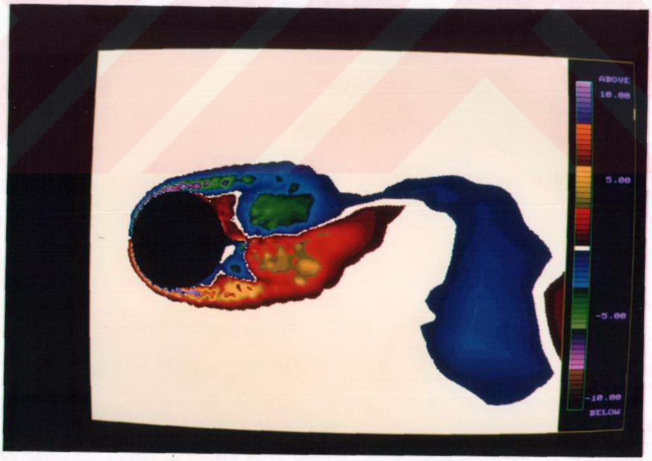

(b)

(For legend see page 71)

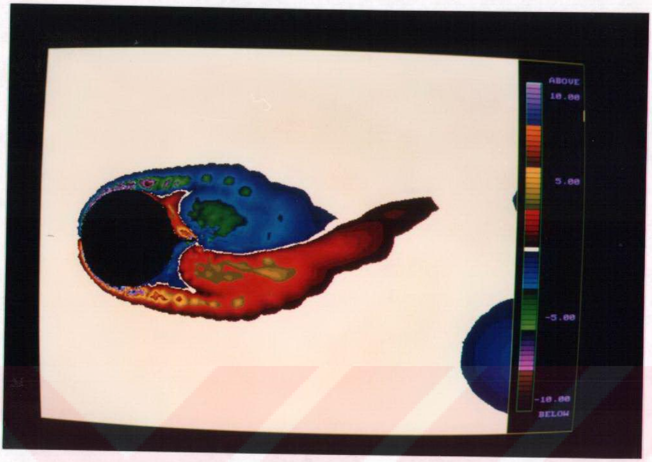

(c)

(d)

(For legend see next page)

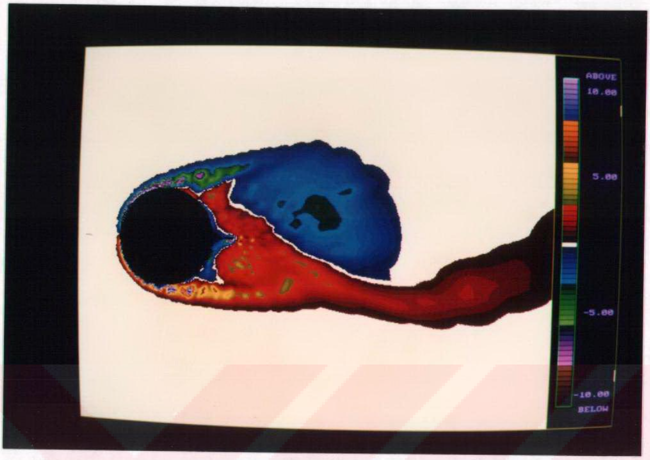

(e)

Figure 4.16 Color coded vorticity distributions for L/D=0.25 corresponding to Fig 4.15

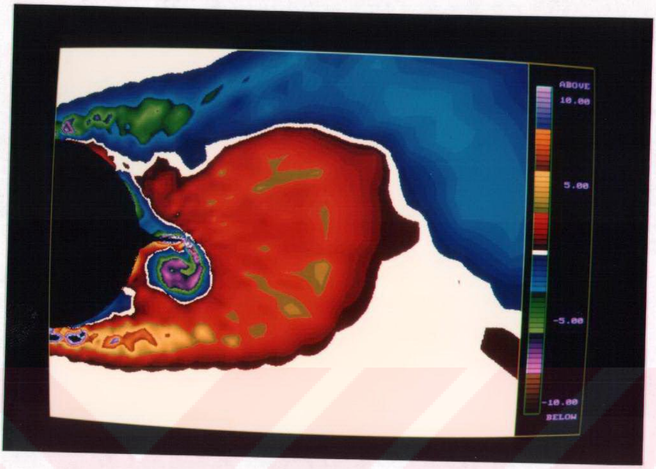

(a)

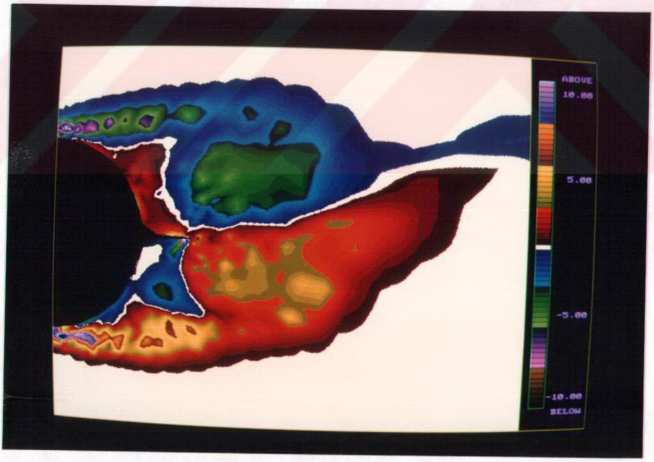

(b)

(For legend see page 74)

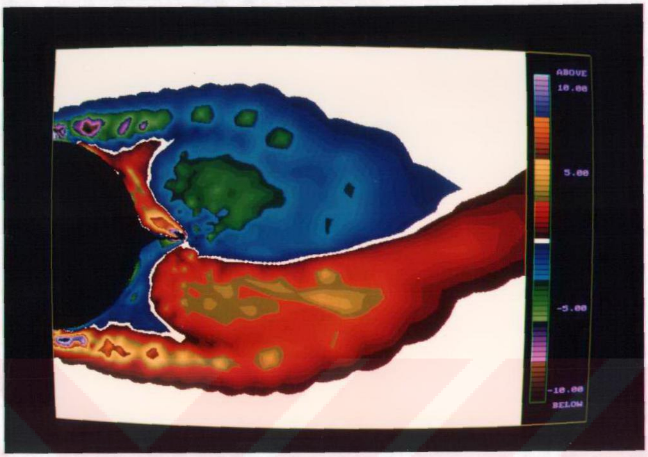

(c)

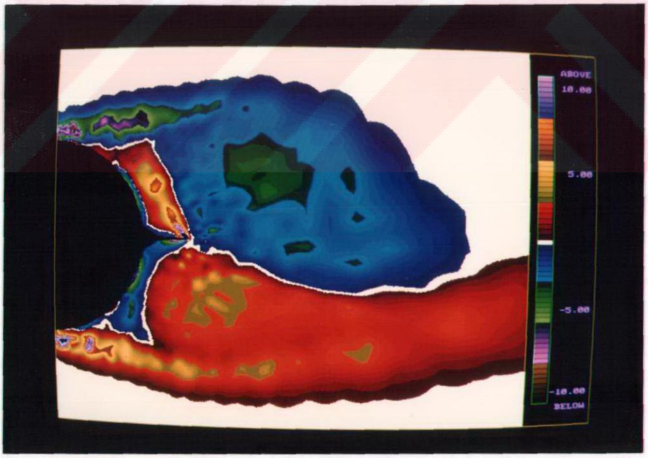

(d)

(For legend see next page)

(e)

Figure 4.17 Color coded vorticity distributions for L/D=0.25 (close–up views)

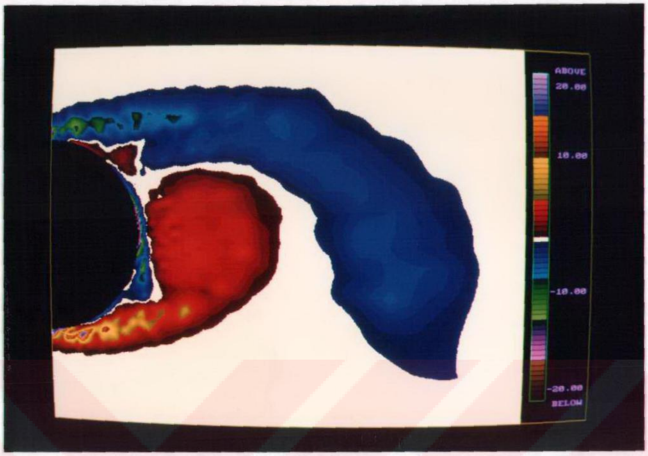

(a)

(b)

(For legend see page 78)

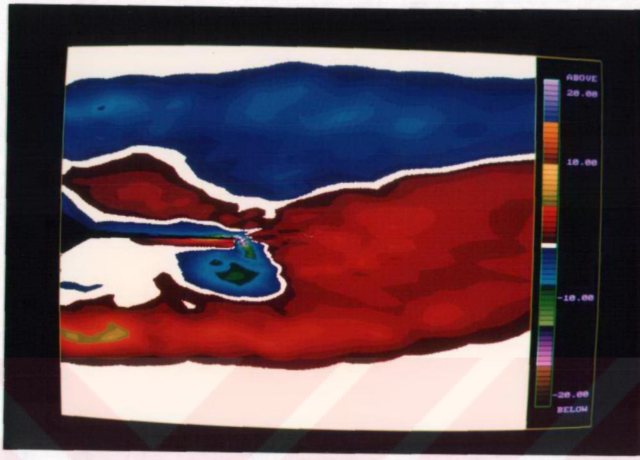

(c)

(d)

(For legend see page 78)

(e)

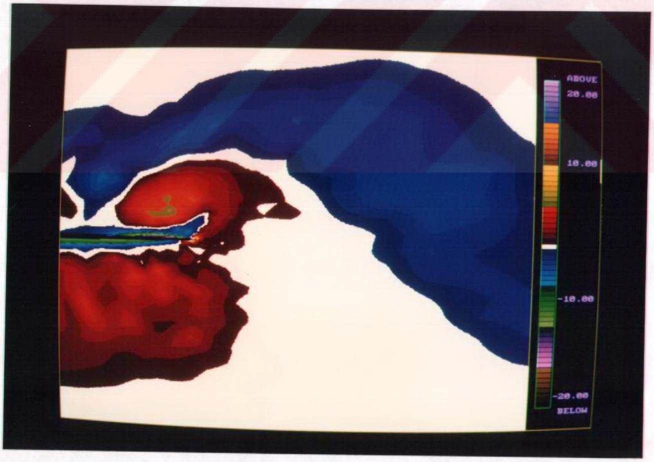

(f)

(For legend see page 78)

(g)

Figure 4.18 Color coded vorticity distributions at the tip of the plate as a function of the splitter plate length.

REFERENCES

[1] Schilichting,H., Boundary Layer Theory, 7th edition, McGraw& Hill Co., 1979

[2] Tritton,D.J.,Physical Fluid Dynamics, Von Nostrand Reinhold Co., 1977

[3] Karman, T.V., Ueber den Mechanicmus des Widerstandes den ein Bewegter Koerper in Einer Fluessigkeit Erfahert,Gottinger Nachrichten math–phys, Kl 547 1911

[4] Blevins,R.D., Flow–Induced Vibration Von Nostrand Reinhold Co., 1974

[5] Roshko, A., On the Drag and Shedding Frequency of Two–Dimensional Bluff Bodies, National Advisory Committee For Aeronautics, Technical Note 3169, 1954

[6] Abernathy,F.H. and Kronauer,R.E., The Formation of Vortex Streets,JFM , vol. 13, pp 1–20 ,1962

[7] Gerrard,J.H., The Mechanics of the Formation Region of Vortices Behind Bluff Bodies,JFM,vol.25,part 2, pp 401–413,1966

[8] Bloor, M.S.,The Transition to Turbulance in the Wake of a Circular Cylinder, JFM, vol 19, part 2, pp 290–304, 1963

[9] Bloor, M.S. & Gerard, J.H., Measurments on Turbulent Vortices in a Cylinder Wake, JFM, pp 319–342, 1966

[10] Bearman, P.W., A Study of Unsteady Base Flows, Ph.D. Thesis, Univ. of Cambridge, 1965

[11] Ünal,M.F. & Rockwell,D.,On Vortex Formation From a Cylinder Part 1: The Initial Instability,JFM,vol 190, pp 491–512,1988

[12] Bouard,R., & Countanceau, M., The Early Stage of Development of the Wake Behind an Impulsively Started Cylinder for $10 < Re < 10^4$, JFM, vol 101, part 3 , pp 587–607, 1980

[13] Thoman, D.C. & Szewczyk, A.A., Time–Dependent Viscous Flow over a Circular Cylinder, High Speed Computing in Fluid Dynamics, The Physics of Fluids Supplement II, pp 76–86, 1969

[14] Ta Poch Loc, Numerical Analysis of Unsteady Secondary Vortices Generated by an Impulsively Started Circular Cylinder, JFM, vol 100, part 1, pp 111–128, 1980

[15] Braza, M.,Chassaing, P. & Minh, H.H., Numerical Study and Physical Analysis of the Pressure and Velocity Fields in the Near Wake of a Circular Cylinder, JFM, vol 165, pp 79–130, 1986

[16] Gerrard, J.H., A Disturbance–sensitive Reynolds Number Range of the Flow past a Circular Cylinder, JFM, vol 22, part 1, pp 187–196, 1965

[17] Peterka, J.A. & Richardson, P.D., Effects of Sound on Separated Flows, JFM, vol 37, part 2, pp 265–287, 1969

[18] Williams, J.E.F. & Zhao, D.C., The Active Control of Vortex Shedding, JFM, part 3, pp 115–122, 1989

[19] Gerich, D. & Eckelmann, H., Influence of End Plates and Free Ends on the Shedding Frequency of Circular Cylinders, JFM, vol 122, pp 109–121, 1982

[20] Greenway, M.E. & Wood, C.J., The Effects of a Bevelled Trailing Edge on Vortex Shedding and Vibration, JFM, vol 61, part 2, pp 323–335, 1973

[21] Strykowski, P.S. & Sreenivosañ, K.R., On the Formation and Suppression of Vortex Shedding at Low Reynolds Numbers, JFM, vol 218, pp 71–107, 1990

[22] Yılmaz, A., Modifications of Wakes From Bluff Bodies: Inviscid and Viscous Discrete Vortex Methods, M.Sc. Thesis, Istanbul Technical University, 1990

[23] Roshko, A., On the Wake and Drag of Bluff Bodies, Journal of Aeronautical Sciences, pp 124–132, 1955

[24] Ünal,M.F. & Rockwell,D.,On Vortex Formation From a Cylinder Part 2: Control by Splitter Plate Interference,JFM,vol 190, pp 513–529,1988

[25] Smith,C.A., Karamcheti,K., Aerodynamic Sound Generation due to the Interaction of an Unsteady Wake with a Rigid Surface, AIAA, paper, No 75–454 Second Aeroacoustics Conference March 1975

[26] Bearman,P.W., Investigation of the Flow Behind a Two Dimensional Model with a Blunt Trailing Edge and Fitted with Splitter Plates ,JFM ,vol. 21, part 2, pp 241–255,1965

[27] Apelt, C.J., West, G.S. & Szewczyk, A.A., The Effects of Wake Splitter Plates on the Flow Past a Circular Cylinder in the Range $10^4 < Re < 5 \times 10^4$, JFM, vol 61, part 1, pp 187–198, 1973

[28] Sarpkaya, T., Computational Methods with Vortices–The 1988 Freeman Scholar Lecture, Journal of Fluids and Engineering, vol 111/5, 1989

[29] Clements, R.R., An Inviscid Model of Two Dimensional Vortex Shedding, JFM, vol 57, part 2, pp 321–336, 1973

[30] Sarpkaya, T. & Schoaff, L., Inviscid Model of Two Dimensional Vortex Shedding by a Circular Cylinder, AIAA Journal, vol 17, No 11, pp 1193–1200, 1979

[31] Kamemoto, K. & Bearman, P.W., The Importance of Time Step Size and Initial Vortex Position in Modelling Flows with Discrete Vortices, Imperial College Aero Report 78–108, 1978

[32] Deffenbaugh, F.D. & Marshall, F.J., The Development of the Flow about an Impulsively Started Cylinder, AIAA Journal, vol 14, pp 908–913, 1976

[33] Sarpkaya, T., An Analytical Study of Separated Flow about Circular Cylinders, Journal of Basic Engineering, Transaction of ASME, pp 511–520, 1968

[34] Spalart, P.R. & Leonard, A., Computation of Separated Flows by a Vortex Tracing Algorithm, AIAA 14th Fluid and Plasma Dynamics Conference, Palo Alto, 1981

[35] Park, W.C. & Higuchi, H., Computation of Flow past Single and Multiple Bluff Bodies by a Vortex Tracing Method, University of Minnesota Supercomputer Intitute, UMSI 89/88, 1989

[36] Inamuro, T., Adachi, T., & Sakata, H., A Numerical Analysis of Unsteady Separated Flow by Vortex Shedding Model, Bulletin of JSME, vol 26, num 222, pp 2106–2112, 1983

[37] Chorin,A.J., Numerical Study of Slightly Viscous Flow , JFM ,vol. 57 ,part 4, pp 785–796, 1973

[38] Christiansen, J.P., Numerical Simulation of Hydromechanics by the Method of Point Vortices, Journal of Computational Physics, vol 13, pp 363–379, 1973

[39] Stansby, P.K. & Dixon, A.G., Simulation of Flows Around Cylinder by a Lagrangian Vortex Scheme, Applied Ocean Research, vol 5, No 3, pp 167–178, 1983

[40] Smith, P.A. & Stansby, P.K., Impulsively Started Flow around a Circular Cylinder by the Vortex Method, JFM, vol 194, pp 45-77, 1988

[41] Benson, M.G., Bellamy–Knights, P.G. & Gerrard, J.H., A Viscous Splitting Algorithm Applied to Low Reynolds Numbers Flows Round a Circular Cylinder, Journal of Fluids and Structures 3, pp 439–479, 1989

[42] Vada, T., Nestegård, A. & Skomedal, N., Simulation of Viscous Flow , Around a Circular Cylinder in the Boundary Layer near a Wall, Journal of Fluids and Structures, 3, pp 579–594, 1989

[43] Graham,J.M.R. & Cozens,P.D., Vortex Shedding from Edges Including Viscous Effects, Fluid Dynamics Research, vol 3, pp 111-114,1988

[44] White, F.M., Viscous Fluid Flow, McGraw–Hill Book Company, pp 68–69, 1974

[45] Roache,P.J.,Computational Fluid Dynamics,Hermosa Publishers,1972

[46] Temperton, C., Direct Methods for the Solution of the Discrete Poisson Equation: Some Comparisons, Journal of Computational Physics 31, pp 1–20, 1979

[47] Çete, A.R., The Effect of Splitter Plate on the Wake of a Circular Cylinder, Discrete Vortex Method, Graduation Thesis, Istanbul Technical University, 1989

[48] Wu, J.C., Theory for Aerodynamic Force and Moment in Viscous Flow, AIAA J, 19, no 4, 1981

[49] Young, J.A., "Viscous Flow Around Vortex Shedding Flowmeters: A Discrete Vortex Model",Ph.D. Thesis, Faculty of Engineering, University of London, 1989

[50] Franke, R., Rodi, W. & Schönung, B., Numerical Calculation of Laminar Vortex–Shedding Flow Past Cylinders, Journal of Wind Engineering and Industrial Aerodynamics, 35, pp 237–257, 1990

[51] Behr, M., Liou, J., Shih, R. & Tezduyar, T.E., Vorticity Stream–function Formulation of Unsteady Incompressible Flow Past a Cylinder: Sensitivity of the Computed Flow Field to the Location of the Outflow Boundary, International Journal for Numerical Methods in Fluids, vol 12, pp 323–342, 1991

[52] Sun, Y., Shen, S. & Chen, N., A Numerical Study of the Response of the Laminar Unsteady Separated Flow about a Circular Cylinder to Changes of Boundary Conditions, DLR, Institut für Theoretische Strömungsmechanik, 1990

[53] Cheer, A.Y., Unsteady Separated Wake Behind an Impulsively Started Cylinder in Slightly Viscous Fluid, JFM, vol 201, pp 485–505, 1989

[54] Jain, P.C. & Rao, K.S., Numerical Solution of Unsteady Viscous Incompressible Fluid Flow Past a Circular Cylinder, High Speed Computing in Fluid Dynamics, Physics of Fluids Supplement II, pp 57–64, 1969

[55] Son, J.S. & Hanratty, T.J., Numerical Solution for the Flow around a Cylinder at Reynolds numbers of 40, 200 and 500, JFM, vol 35, pp 369–386, 1969

[56] Engelman, M.S. & Jamnia, M.A., Transient Flow Past a Circular Cylinder : A Benchmark Solution, International Journal for Numerical Methods in Fluids, vol 11, pp 985–1000, 1990

[57] Song, C.C.S. & Yuan, M., Simulation of Vortex–Shedding Flow about a Circular Cylinder at High Reynolds Numbers, Journal of Fluids Engineering, vol 112, pp 155–163, 1990

[58] Kawai,H., Discrete Vortex Simulation for Flow around a Circular Cylinder with a Splitter Plate, Journal of Wind Engineering and Industrial Aerodynamics, 33, pp 153–160, 1990

APPENDIX A

Finite Difference Forms on Rectangular Mesh

The basis of the approximation of flow equations used in this study is the Eulerian concept of discretising the flow field onto a mesh to calculate quantities such as velocity and circulation . According to this concept, equations are derived for a rectangular mesh and each term in flow equations, used for the diffusion and convection processes are obtained in discretized form. First and second order difference formulae are used for constant mesh spacing in –x direction and expanding, unequal, mesh spacing in –y direction. Also the Fourier transformation of Poisson's equation is taken in –x direction. The discretized forms can be derived by using Taylor series expansion. In general, let f(x) be a function whose differences are required to be established at a point "p", provided that f_{p-1}, f_p, f_{p+1} are given.

For the unequal mesh spacing, definition of mesh intervals is ;

$$\Delta y_p = y_{p+1} - y_p \tag{A.1}$$

$$\Delta y_{p-1} = y_p - y_{p-1} \tag{A.2}$$

and the ratio of these is

$$s = \frac{\Delta y_p}{\Delta y_{p-1}} \tag{A.3}$$

Taylor series with the definitions above are:

$$f_{p+1} = f_p + f'_p \Delta y_p + \frac{1}{2} f''_p \Delta y_p^2 + \frac{1}{6} f'''_p \Delta y_p^2 + ... \qquad (A.4)$$

$$f_{p-1} = f_p - f'_p \Delta y_{p-1} + \frac{1}{2} f''_p \Delta y_{p-1}^2 + \frac{1}{6} f'''_p \Delta y_{p-1}^2 + ... \qquad (A.5)$$

Subtracting equation (A.4) from equation (A.5) gives

$$f'_p = \frac{f_{p+1} - fp - 1}{\Delta y_p + \Delta y_{p-1}} + \frac{1}{2} f''_p \frac{\Delta y_p}{s}(1-s) + O(\Delta y_p)^2 \qquad (A.6)$$

Taking only the first term in the right hand side gives a first order accuracy; for s=1 accuracy is second order. A second order accurate expression for f''_p obtained from A.4 and A.5 is as follows

$$f''_p = \frac{2s}{s+1} \frac{s f_{p-1} - (1+s) f_p + f_{p+1}}{\Delta y_p^2} + O(\Delta y_p)^3 \qquad (A.7)$$

From these foregoing expressions it is now easy to discretise the equations in the finite difference form proper for the solution on a rectangular mesh in cartesian coordinates. Thus the diffusion equation in two-dimension becomes;

$$\omega_{i,j}^k = \omega_{i,j}^n + \Delta t \nu \left[\frac{\omega_{i-1,j}^n - 2\omega_{i,j}^n + \omega_{i+1,j}^n}{\Delta x_i^2} \right.$$

$$\left. + \frac{2s}{(s+1)} \frac{s\omega_{i,j-1}^n - (1+s)\omega_{i,j}^n + \omega_{i,j+1}^n}{\Delta y_j^2} \right] \left| \frac{\partial \zeta}{\partial z} \right|_{i,j}^2 \qquad (A.8)$$

where $|\frac{d\xi}{dz}|_{i,j}^2$ term is the transformation modulus, "n" refers the condition at time "t" and "k" refers to the intermediate condition between "t" and "$t + \Delta t$". In fact, the method uses mostly the circulation values as mentioned before. Mesh circulation is defined here as;

$$\Gamma_{i,j} = \omega_{i,j} \Delta x_i \frac{(\Delta y_j + \Delta y_{j-1})}{2} \qquad (A.9)$$

then in terms of circulation the diffusion equation can be rewritten as ;